In-vitro three dimensional spheriods for personalized radiation therapy

A Dissertation Presented

By

Yuting Qiu

to

The Department of Chemical Engineering

In fulfillment of the requirements
For the degree of

Doctor of Philosophy

In the field of

Chemical Engineering

Northeastern University
Boston, Massachusetts

July 16th, 2018

ACKNOWLEDGEMENT

I would like to express my heartfelt appreciation and gratitude to everyone who has helped and supported me during my time here at Northeastern and throughout my life in the events leading to my decision to undertake a Ph.D. degree in chemical engineering.

First of all, I would like to thank Professor Ming Su for letting me continue working in his lab after I finished the study in chemistry and chemical biology department. Professor Su gives me freedom to pursue the projects that I am interested in, and is very willing to spend time out of his busy days to reply to our emails quickly, and to review our paper drafts. I would also show my heartfelt thanks to my committee members, Professor Sidi Bencherif, Professor Ryan Koppes from Chemical Engineering Department, Professor Qiaobing Xu from Tufts University, for their time and their valuable discussions on my research. To my lab members, I specially thank Seng Kah Ng for his guidance on doing cell assays. I would like to express my thanks to Marissa Puzan from Dr. Koppes's group for her time to help me with the modification of the thesis, she is always there to support me! I would also like to express my special thanks to Dr. Shi from bioengineering department for his encouragement. Last, I specially thank Rob Eagan for his dedicated work on helping us, as well as Bill Fowle and Wentao Liang for their guidance on operating electron microscopes.

To my parents, I always feel grateful for their support. They give me a lot of freedom to choose the way I would like to take. I would like to thank all of my wonderful mends both in China and in US for their support and encouragement. Last but not least, I would like to extend my immense gratitude to the faculty and staff of the College of Engineering and the Department of Chemical Engineering at Northeastern University for

providing me with facilities and allowing me this great opportunity to further my education.

This research was fully funded by Northeastern University.

ABSTRACT

X-ray radiation therapy can be used for to treat cancer for primary therapy of localized tumors and for adjuvant and palliative therapy to relieve symptoms from later stage or metastatic diseases. This proposal describes the use of radiation enhance DNA damage of cancer cells in 3D microtissues. The main objective is 3D Microtissues as *in-vitro* model for radiation induced cell damage. Here we describe a high-throughput and personalized approach to test *in-vitro* toxicity in three-dimensional (3D) microtissue array, where microtissues are formed by seeding cells in nonsticky microwells, and cells are allowed to aggregate and grow into microtissues with defined size and shape. When X-ray radiation dose increases, more photoelectrons and Auger electrons are generated, which cause water ionization, and lead to formation of free radicals that damage DNA of cancer cells.

I have finished the aims at detecting the kinetics behavior of 3D microtissues in matrigel dependence on different sizes. The radiation damage to 3D microtissues under hypoxic condition. The 3D microtissues have been studied in physical properties. The damaged to 3D microtissues induced by X-ray radiation have been detected on cellular level using a panel of assays. The enhanced radiation damage to cells is confirmed at single cell level, chromosome level, protein level by single cell Halo Chip assay, micronucleus assay and measuring the expression of DNA double strand repair protein (γ-H2AX), respectively. Migration of 3D microtissues will be studied in different concentration of alginate gel. Animal test of 3D stem cells transplantation will be explored as well.

TABLE OF CONTENTS

LIST OF FIGURES

LIST OF TABLES

1.0 Introduction

Current treatments for cancer include chemotherapy, surgery and radiation [1]. Radiation therapy and ionizing x - ray therapy is an important part of cancer treatment. It can be used for primary treatment of local tumors and can be used for adjuvant and palliative care to alleviate the symptoms of advanced metastatic disease. The purpose of radiotherapy is to eliminate the tumor by laser treatment [2,3]. Lasers can produce free radicals that destroy the cellular components, including DNA strands. Even if it is mixed with a normal tumor, it can kill the tumor, which is the most important advantage of radiotherapy. Therefore, more than 60% of cancer patients choose radiotherapy [4-6]. But we also know that therapeutic doses used in radiotherapy can be harmful or kill close to normal tissue. Various chemicals and nanoparticles have been tested as a radiosensitizer to enhance the effect of radiotherapy on tumors. Have improved accuracy and efficiency of the dose delivery and the latest progress of targeted groups combined with physics, biology, and clinical radiation therapy, radiation therapy, a big challenge, for example, it is still provided accurate access while minimizing damage to normal tissue [7-11]. Once it is absorbed, X-ray photonic photoelectrons and auger electrons can be produced in radiotherapy, which can cause ionization of water molecules, and then it produces a large number of reactive free radicals. Free radicals can spread through the chain reaction inside the cell, and then by extracting the hydrogen atoms from the ribosaccharides, resulting in the split of the DNA skeleton, causing damage to the mitochondrial DNA [12-14].

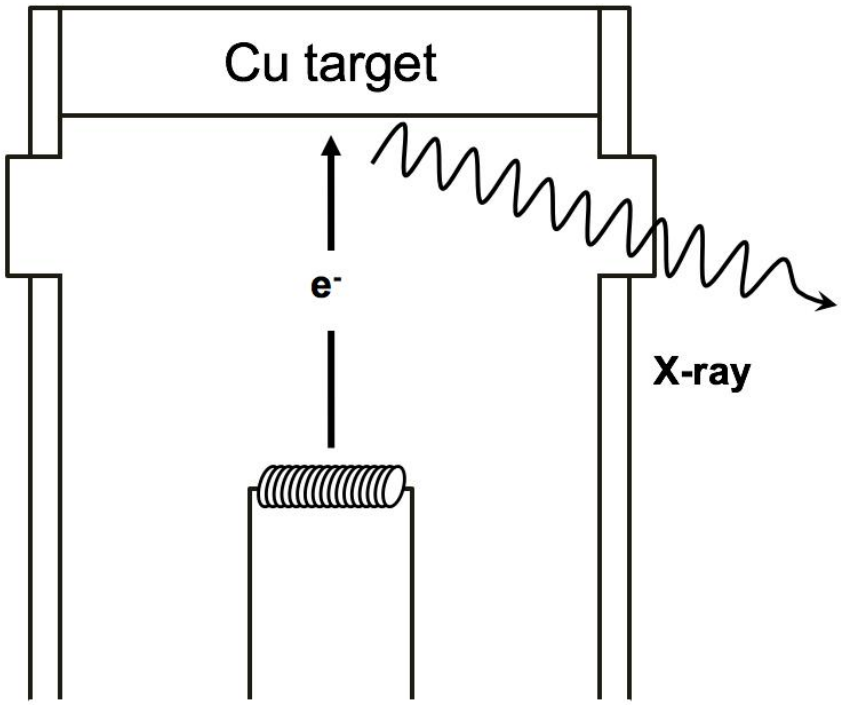

Figure 1: X-ray generation from high energy electron beam.

There are many advantages using 2D cell cultures, one of these is much easier environmental control, cell observation, measurement, as well as eventual manipulation in comparison than 3D cultures [15-19].

Has many limitations, for example, in the body systems (such as changes in gene expression), compatibility with the body system is reduced, such as drug sensitivity increases, in clinical and basic research, exposed to the surface of the obstacle [20]. In many solid tissue tumors, there is also the challenge of producing cytotoxic T cells to migrate or infiltrate the tumor site, thus determining how tumor cells escape all cells [21-22]. However, as we know, not all tumor types respond to immunotherapy. In both of these challenges, the 3 d printing tumors will provide excellent model to study the mechanical immunization and the interaction between tumor cells and test new biological agents, we know that the normal X-ray radiation therapy can be widely accept local

tumor, late or metastatic cancer symptoms can breath a sigh of relief. Therefore, one of the challenges of radiotherapy is that the radiation dose we use in the treatment conditions can damage the normal tissue in the patient [23-24].

This problem is mainly caused by two factors: the energy deposition selectivity of tumor and the sensitivity of tumor to radiation injury after treatment. Beam installation technology, such as, image guided radiotherapy and intensity-modulated radiation therapy, as well as the proton therapy has been used to improve the energy deposition in the tumor is less, the dose in the normal cells, at the same time, it can make it larger doses of the cancer cells. The radiation beams we use can respond to tumors in multiple directions in a room to avoid the path of the normal cells and the human body. Using various kinds of beamlets of various intensities, the dose of tumor cells can be maximized to conform to the morphology of human tumor cells [25].

Radiosensitizers such as nanoparticle medicine of the more heavier elements targeted at the tumor cell sites, it has been used to enhance the deposition of radiation energy[26]. With the difference in the repaired ability of cancer with the normal cells. It has also been utilized in our treatment, where the total radiation dose is fractionated over

time to allow the normal cells to recover from damage after X-ray irradation, while at the same tine, the cancer cells that are radioresistive in the first period time, it moved into a radiosensitive phase of the cell cycle in the next period, it can be deteced using flow cytomytry[27]. It has been deteced that radiosensitivity varies to a great extent across tumor types, while at the same time, it has been found between patients bearing the same types of tumor. There is a significant need for tools to predict the efficacy of radiation therapy in individual patients. It has called us attaction that the selection of radiation therapy in a treatment plan for a particular patient is caused by the clinical and pathological features of tumors in human, here is a goal of personalized radiation therapy is to identify patients who are sensitive to radiation therapy where we know the method has different effects on patients, but when the low-risk patients can get the treatment additional benefits from the radiation therapy, while at the same time, high risk ones will be recommended to undergo surgery[28]. Meanwhile, at the same time, the used personalized approach can provide alternated dosing schedules or plans for differnet patients to reduce the total radiation dose, so it can make minimize the effect on patients. The radiosensitivity of a tumor can be assessed by evaluating the gene of patinets that

network through a systems biology approach, at the same time, biomarkers now is derived from tumors from patients can also be used to predict radiation sensitivity as personalized, although outcomes of the prediction are heterogeneous as a result of gene expression due to epigenetic control in human body[29-32].

As we know, in vitro grown mammalian cells can be used to detect with the effects of radiation on cancer cells in patinets. However, cells from two-dimensional (2D) monolayer cultures do not respond to radiation as tissues, it can not mimic the real tissue in human body [33-35]. Cells in three-dimensional (3D) clusters, aggregates are in an environment close to physiological conditions and can mimic the tissue architectures, with the functions of human being, at the same time, these aggregated cells have shown higher stability than those from a 2D culture based on the result. Despite their great benefits over 2D models, as well as the 3D tissue models, it still encounters several limitations. Such as, one of their limitations is in the requirement of large numbers of cells and various cell types integrated into complex configurations, second one, ECM-derived matrices might have batch-to-batch variability in tomor's biological characteristics. Many studies has used the standardized microfluidics or microarray-based especailly single cell array based HTS for drug discovery, also for toxicity testing

reported that we used of ECM components for natural scaffolds were often not consistent with the result. Thirdly, we know the 3D culture can be generally very expensive for large-scale studie, espencailly for the high-throughput assays. Last not least, vascularization in 3D models remains an unsolved problem since it is the subject of active research, of which plays a important role in tissue growth and survival as well as in drug delivery. The core of tissue spheroids we use might create a hypoxic environment or limit the diffusion of compounds into the core, which is different from normal tissues. These limited shortcomings are mainly important due to a low level of biomimetic organization of the heterocellular environment, it can not mimic the real tissue in human body, also instability and low repeatability of the developed 3D models. Biomimetically developed miniaturized tissue modelsl, it has met these limitations, by contrast with other tissues, might be fabricated by the accurate deposition of cells and ECM components to recapitulate the native architecture of tissues, at the same time, it is highly feasible using 3D bioprinting as compared[36-40].

A panel of X-ray radiation techniques as resported have been used to minimize dose on normal cells or maximize dose on cancer cells in the research[41-43]. To allow

the normal tissue become healthy after treatment, while at the same time, cancer cells that are relatively radioresistive in the first treatment move into a relatively radiosensitive phase of cell cycle in the next treatment, which lead to the next treatment in clinical treatment, the dose can be fractionated over space to intersect at tumors from several directions to spare normal cells along beam path as reported[44-45]. We know the image-guided radiation therapy as well as the intensity-modulated radiation therapy could be used to maximize X-ray doses on tumors in human body and make the structure of tumor's 3D shapes with multiple beam lets of various intensity, at the same time.

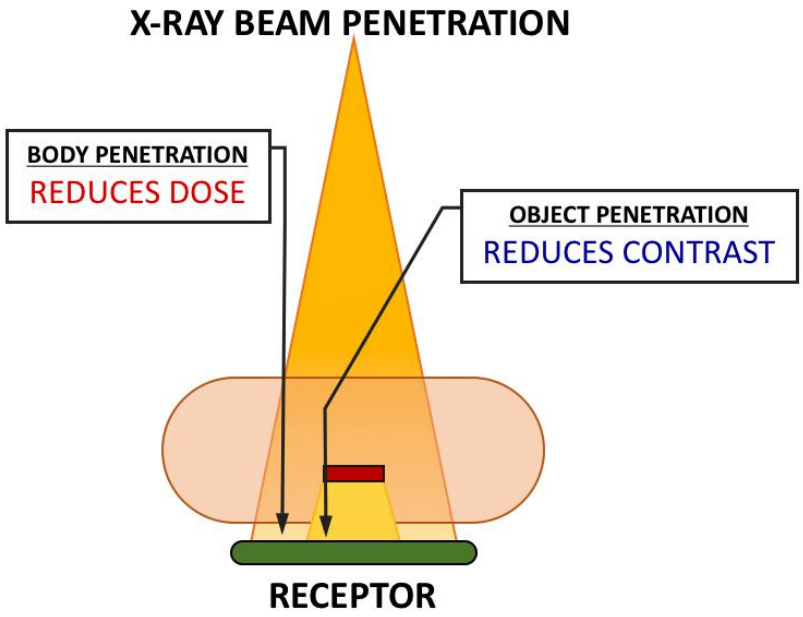

Figure 2: X-ray radiation therapy on human body.

Radioprotective drugs, now it widely used in as free radical scavengers to protect normal cells from damage after radiation. There are radiosensitizers such as oxygen, oxygen carrying blood substitutes as well as radiosensitive drugs which have been used to decrease the effects of given X-ray doses. As we know, the avascular three-

dimensional (3D) microtissue culture systems have been widely used to evaluate toxicities of drug candidates such as anticancer drugs. Three-dimensional micro and millimeter tissues we used can develop morphological, physiological characteristics similar to those of *in vivo* grown tissues in human body. So it is between that 3D tumor microtissue-based toxicity assays which can fill the knowledge gap and in vitro 2D cell assay and *in vivo* animal tests. Three-dimensional tumor microtissue could also acquire clinically relevant multicellular resistance to apoptosis-inducing drugs which can mimic chemoresistance of solid tumors in human body[46-48]. There are many methods that have been developed to make 3D microtissues for example, the surface patterning, like hanging drop, micromicrotissue chips, liquid-overlay methods, spinning, microfluidics, and printing. Each method has its own advantages and limitations. For example, spinner flask technique can be used for large-scale culturing and maintaining microtissues with different conditions after a long time [49-50]. However, it is necessary to transfer the microtissues to stationary culture systems before running a toxicity assay. Such transfer could change microtissues morphology or damage its structure, making accurate microtissue monitoring if impossible as predict. There ae hanging drop techniques can form relatively uniform microtissue and are cost-effective, but a transfer step is also required before the toxicity assay, which is cumbersome and is counterproductive to large-scale screening; also, we know non adhesive dishes can result in formation of multiple microtissues with a large board of different size range, this require further sorting and are not suitable for screening. As we know, it is also the size-defined 3D microtissues can be produced by some gravity-enforced assembly methods, but cellular organelles within the microtissue are potentially damaged due to shear stress.

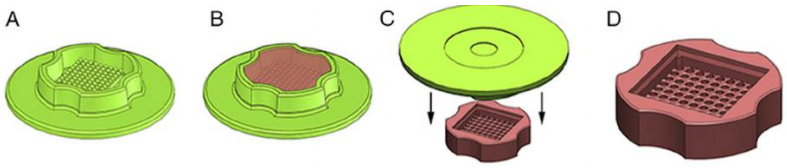

Figure 3: Method to generate micro-mould.

Here, therefore, this research describes a method that uses radiation therapy to cancer cells in 3D microtissues [51-53]. The 3D microtissues are generated by culturing cancer cells in agarose microwells. Where upon large level dose of X-ray irradiation, a higher level of DNA damage can be induced in cells in microtissues. The enhanced DNA damage in cells in 3D microtissues has been confirmed with single cell array based Haloassay, expression of DNA repair proteins, as well as micronucleus assay.

2.0 Critical Literature Review

2.1 Cancer

2.1.1 Cancer Prevalence

Cancer is the biggest disease in the world, and human cells grow and divide to form new cells because the human body needs them [54-55]. When cells become more and more abnormal, old or damaged cells survive when they die, and new cells form when they don't need them. These extra cells can divide without stopping and can form tumors. Many cancers form solid tumors in the body, which is a large number of tissues [56-57]. As far as we know, leukemia does not normally form solid tumors. But unlike malignant tumors, benign tumors do not spread or invade nearby tissues [58-59]. However, benign tumors can sometimes be very large in the human body. When transferred to other places, they usually don't grow back, and malignant tumors sometimes. Unlike most benign tumors of the human body, a benign brain tumor may be life-threatening and then a metacomal tumor [60-62].

In all types of cancer, many of the cells in the body begin to divide, not stop and spread around the body. Cancer cells can be activated almost anywhere in the body, which is made up of trillions of cells. Usually, as human needs. When human cells need them, they grow and divide, forming new cells. When cells grow old or damaged, they die, and new cells take their place. However, when cancer occurs, it sometimes splits into fragments. When cells become more and more abnormal, old or damaged cells survive when they die, and new cells form when they are not needed. These extra cells can divide without stopping and can form tumors. Many cancers form solid tumors in the body, which is a large number of tissues. Cancer in the blood, such as leukemia, usually does

not form solid tumors. Cancerous tumors are malignant, meaning they can diffuse or invade nearby tissues. In addition, as the tumor grows in after a period of time, some cancer cells can spread through the blood or lymph system block and into the body, far away, to form a new tumor, away from the initial formation of the tumor. But unlike malignant tumors, benign tumors do not spread or invade nearby tissues. However, benign tumors can sometimes be very large in the human body. When transferred to other places, they usually don't grow back, and malignant tumors sometimes. Unlike benign tumors in other parts of the body, a benign brain tumor can be life-threatening and become a malignant tumor.

2.1.2 Cancer Generation

We know that the tumor stromal cells are the secretion of cytokines and growth factors gradient, it may help change cell proliferation, as well as instructions to promote the development of tumor cell migration, dissemination and attack. We know that with the spread of the tumor, oxygen demand cannot be satisfied by the existing tissue vascular system in order to change the energy [63-64]. What we do know is that hypoxia is also associated with resistance, because hypoxic stress affects the cell cycle, and slow circulating cells are thought to be the least affected by the treatment of the cell cycle. We note that they will affect the reaction of the drug, it will also affect the regulation of cell proliferation and ECM production of genes, cell adhesion and cell infiltration, these genes are induced by hypoxia-inducible factor (HIF) of the family. Angiogenesis growth eased to some extent caused by lack of oxygen, but lack of normal artery blood capillary angiogenesis of tumor classification arrangement, which may lead to leakage of intercellular, blood and brain, and low efficiency of oxygen transfer [65-68].

Also, the metastatic cancer has the same name and the same type of cancer cells as the original, the name of metastatic cancer is the same as that of cancer cells, and there are primary or primary cancers. For example, metastatic tumors that can spread to the lungs are metastatic breast cancers, not just lung cancer [69-72], our goal is to treat cancer and protect normal tissue.

Tumor stromal cells and gradient secreted cytokines and growth factors, these factors can promote cell proliferation, also can promote cell migration, promote the development of tumor, dissemination and attack. We know that when the tumor spreads, their energy and oxygen demand cannot be met by the existing tissue vascular system. Hypoxia is also associated with drug resistance, because hypoxic stress affects the cell cycle, and slow circulating cells are thought to be the least affected by the treatment of the cell cycle. They can affect the reaction of the drug, but also involved in regulating cell proliferation, gene, cell adhesion and cell infiltration of the ECM production increases, these genes induced by hypoxia-inducible factor (HIF) family of transcription factors. Angiogenesis in a certain extent, ease the growth induced by hypoxia, but lack of normal artery tumor blood vessels - ranking of capillaries, which may lead to leakage of intercellular, blood and brain, oxygen, and low efficiency.

Therefore, in the growing mass, there are some areas of hypoxia, and some cancer cells are deprived of oxygen conditions. In the process of aerobic and anaerobic glycolysis, hydrogen (H+) ions generated by tumor cells, glutamine hydrolysis, and ATP hydrolysis are transferred to the extracellular environment to form the human acidic tumor microenvironment. These acidic environments are considered to be licensed for tumor invasion and continuous metastasis, by inducing cell death and ECM degradation

in surrounding normal tissue. Extracellular matrix on the biochemical and physical can simulate organs in the body of the three-dimensional (3 d) culture system, is widely used in the breast, prostate, the formation of the salivary gland and kidney normal epithelial organs. In addition, drug research on the three-dimensional spheres involving endothelial cells has been widely used to assess the potential of pro and anti-angiogenesis in drugs targeting tumor blood vessels. In these bionic systems, the cells adopt physiological morphology and obtain corresponding cellular signals. The three-dimensional culture model can also be used to summarize the non-biological and biological components of tumor ecosystem. The non-living components of space and time gradient chemical substances, such as oxygen tension, and mechanical signal can use the application from microuidics strong engineering, electrospinning, so the lithography, the ECM biological components (such as cell interaction environment and the abnormity can approximate using bionic system platform and cooperation culture. Although the traditional two-dimensional tissue culture system has made great contributions to the development of cancer biology, the cancer cells will encounter a variety of three-dimensional topography and structure in the body. The three-dimensional culture model deconstructs the complexity of cancer by reorganizing the emergent and demographic characteristics of tumor microenvironment. Tumor microenvironment is characterized by cells and biochemical composition, and physical and chemical parameters such as hardness, pH, oxygen tension, complex interaction, such as interstitial pressure is very important to study these factors. Both tumor and stromal cells can produce the gradient of secreted cytokines and growth factors, which can greatly promote cell proliferation and targeted cell migration, and promote tumor progression, transmission and invasion.

Metastatic cancer has the same name and type as primary cancer. For example, metastatic tumors that can spread to the lungs are metastatic breast cancers, not just lung cancer. Under a microscope, metastatic cancer cells are usually the same as the original cancer cells we observe. In addition, metastatic cancer cells and cells in the original cancer usually have some common molecular characteristics, just like certain chromosomal changes. Treatment may help extend the lives of some metastatic cancer patients. In general, the primary goal of the treatment of metastatic cancer is to control the growth of cancer or to reduce the symptoms it causes. Metastatic tumors can cause serious damage to human function, while most people who die from cancer die from metastatic disease worldwide.

2.1.3 Cancer Personallized Treatment

By conducting genetic tests on cancer cells and other normal cells, doctors can find the best treatment for each patient's needs. Personalized medicine is a medical service tailored to the individual characteristics of each patient. Here, we want to overcome the scientific breakthrough we have made about how a person's unique molecular and genetic characteristics make it more susceptible to certain diseases. The same research has also improved our ability to predict which medical methods are safer and more effective for each patient, and which are not [73-77]. As we know, personalized medicine may be seen as an extension of traditional understanding and treatment of disease. Equipped with tools to be more accurate, the doctor can choose a treatment or treatment protocols based on the patient's molecular image, not only can reduce the harmful side effects, to ensure a more successful results, but also can help to control the cost and disease treatment method of "trial and error". Personalized medicine may change

the way we think, identify and manage health problems. It has had an exciting impact on clinical research and patient care, and as our understanding and technology improves, the impact will increase. Personalized cancer treatment is a treatment strategy, and its core is to predict which patients are more likely to respond to specific cancer treatments. This approach is based on the idea that tumor biomarkers are associated with the prognosis of the patient and the tumor response to treatment. In addition, the genetic factors may be related to drug metabolism, drug reaction and drug toxicity. This personalized cancer therapy website is specifically for doctors and patients developed a tool that can be used to assess potential treatment scheme based on specific tumor biomarkers, and based on the cell or assays research related disease model based on system of phenotypic changes [78-79]. Individualized tumor molecular profiles, the location of tumor disease and the characteristics of other patients are potentially used to determine the best individualized treatment regimen. Tumor biomarkers can be DNA, RNA, protein and metabolomics data to predict therapeutic responses. The most recent method, however, is sequencing the tumor's DNA, which could reveal changes in the genome that affect the treatment of cancer. They may have only one or a few main reading - nuclear cytoplasmic strength than tag receptors, such as the host of other information, such as the distribution of receptor model, how to spread the other side of the cell and cell morphology, at the same time acquisition and quantification. The multiple parameter data, and then by multiplex coloring and increasingly sophisticated image analysis software, describes the detailed information of the cell shape and intensity distribution of these data can be merged into a delicate assessment, for example, a compound the overall effect of a system. Phenotypic analysis is a useful method, based on the analysis of the target can't do, such as when the

target is unknown or cannot be isolated in vitro test, and may be used to not only look at the target of interest, and how it affects the whole channel or interested in systems biology target [80-82].

Many insurance plans may not cover the costs of these tests. In addition, some personalized treatments, such as targeted treatments, which can be more expensive in the research as we know, which means that the person would require a higher dose of that drug for it to be effective, what is more, there is someone body may not process a drug as quickly, so it is need to be in personalized treatment [83-85].

Personalized medicine is a gradual approach to cancer treatment. Doctors don't know the genetic changes that occur in cancer cells. Nor do they know how these new cancer treatments work. Targeted therapies may stop working, promising treatments are no longer as effective as they are described. The drug stays in the blood longer and can cause more serious side effects [86-90]. And, more importantly, early and accurate diagnosis of cancer is still a challenging task, because today's many diagnostic technology are low sensitivity, a large number of sample preparation, long turnaround time, lack of diversity, high cost and high misdiagnosis rate [87]. In addition what is more, following the diagnosis by treatment that often involves frequent exposure to high radiation doses, chemotherapy and invasive measures like surgery which prolong patient suffering [88].

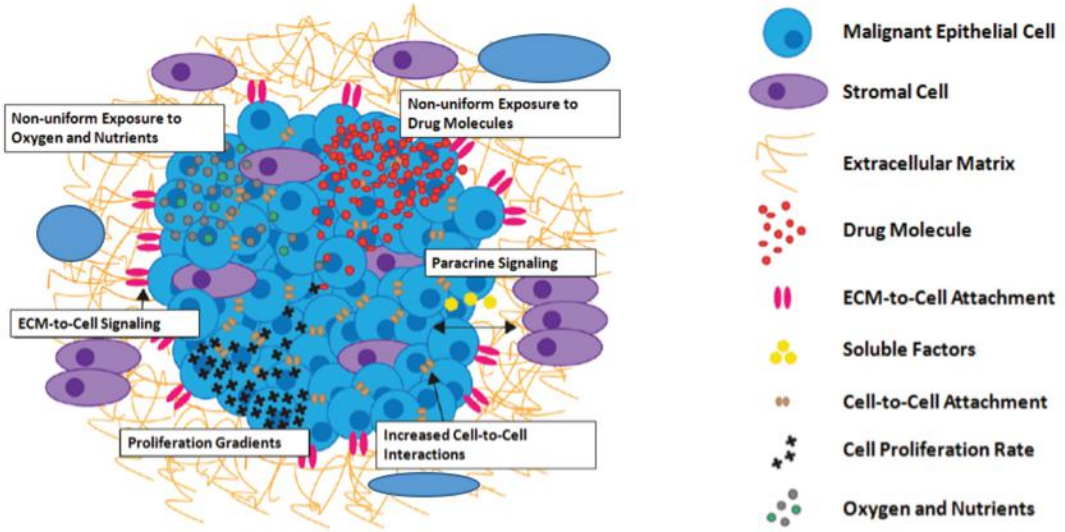

Figure 4: Tumor microenvironment.

2.2 3D Microtissues

2.2.1 Why 3D Microtissues?

In vitro models continuously evolve with more closely mimic and predict biological responses of living organisms. Many novel three dimensional (3D) organotypic models, which resemble from the tissue structure, function as well as disease progression, have been developed [89-90]. However, the application of more complex models and technologies may increase the risk of compromising assay robustness and reproducibility. Consequently, the first developmental stage of cell-based assays is to combine complex tissue models with standard assays, a combination that already provides more physiologically insightful information when compared to two-dimensional (2D) systems [90-93]. Our last goal should be to exploit the full potential of tissue-like *in vitro* models by investigating them with modern assays such as omics and imaging technologies under the biotechnology platform. Furthermore, organotypic models will

allow for a new design of novel assay concepts that utilize the whole tool and useful boxes of models and endpoints [94].

Three-dimensional (3D) cell culture can provide the possibility of maintaining cells in a physiological environment, allowing cells to interact and interact with cells in the extracellular matrix. Extracellular matrix also regulates cell morphology, gene expression, and epigenetic plasticity in the body. Traditional two-dimensional (2 D) rapidly losing the function of the liver, liver culture lead to in vitro and in vivo data consistency between the poor, especially in the heterogeneous metabolic and transporter of activities in the human body. The three-dimensional culture of primary human hepatocytes maintains the long-term survival and maintenance of liver specific function in vitro. In microfluidic device, when there are multiple tissue or organ system are discussed, known as "cell biology chip", "organization chip" or "body chip" in 3 d culture (also known as 3 d micro type, tissues and organs and tissue culture). These platforms can analyze the biochemical and metabolic activities of living cells in functional and organ environments, while allowing high-resolution real-time imaging. We have now demonstrated the integration of electrochemical microsensors into a standardized and customized culture container for single-layer development of 2D cells [95-99].

Cell metabolism was measured in a few days and was quantified in the metabolic response to the addition of drugs. The electrochemical sensor has high time and spatial resolution for unlabelled in-situ measurement. The sensitivity is high enough to be measured in a low micromolar range, defined as zero. The use of enzymes in biosensors provides high selectivity. The sensitivity and linear range of the sensor can be adjusted by different membrane compositions [100-101]. InSphero scientists spent years

to perfect 3 d cell model development technology, so you don't have to worry about looking for cells, and certification or validation of a consistent size, feasibility and the function of the production run. You can confidently accept robust, standardized 3D microstructure models that are automated, easy to use, and can be used as needed [102-105].

Different from 2D cell culture, 3D liver tissue, even after long-term cultivation, retains many functions similar to viruses. This 3D culture is increasingly being applied to the study of liver damage in toxicology that is exposed to drugs. However, these microstructures need to be thoroughly metabolized to understand the impact on cultural behavior. We measured the metabolic parameters of individual hepatocytes by online and continuous electrochemical microsensors. A microsensor platform for lactic acid and oxygen is integrated into a standard 96-orifice plate. Electrochemical microsensors for lactic acid and oxygen allow rapid, accurate and continuous long-term measurement of metabolic parameters in the microwave. The ability to accurately detect the change of small concentrations through a single sphere is the key to its metabolism. The lactic acid content in the culture medium was monitored and accurately quantified for three days from 50 m/m rate and production 5 mh-1[106-108]. Parallel long-term oxygen measurements show that microwaves do not have the conditions for hypoxia or hypoxia. The increase of lactic acid during aerobic metabolism was observed. The dose-dependent reduction of lactic acid was determined by the addition of Bosentan. We found that in toxicological applications, metabolic monitoring produces quantitative, online cellular activity information that can be supplemented and supported by other methods, such as microscopes[109-120]. The experiment shows that in the alternative strategy of animal

experiment, the method of continuously obtaining 3D cell culture metabolism under standard setting can improve the level of the toxicological model in vitro. In tissue engineering, cancer treatment and individualized treatment, it is important to control the microenvironment of this organ culture [121-123].

The number of cells in a sphere or three-dimensional microstructure is usually lower than that of a 2D cell culture, so the expected concentration changes are small. The microfluidic can reduce the total capacity, and the undiluted metabolites are extracted in the medium. However, they are not easily combined with non-adherent three-dimensional microstructures unless they are supported by a solid matrix or trapped in a microstructure. In addition, cells need continuous perfusion or regular exchange of media [124-126]. Many micro system and three-dimensional cell culture, drug screening, introduces the alternatives to traditional culture can range from the ship as a microtiter plate or hanging drop system, add microfluidics, at the same time, special microfluidic platform, can also be allowed to capture and perfusion, and even form cell clut globule. Standardized Settings allow for compatibility with tablet readers and other high-throughput devices, while microfluidic devices allow for smaller volumes and thus more effective medium exchange or drug exposure. These systems will prove to be very important in vitro pharmacokinetics research, can improve the study of inference in vivo drug affect drug screening application of proven analysis microtissue dyeing size, life/death, fluorescent or colorimetric method, each performance in situ or from supernatant fluid. Electrochemical sensors are rarely combined with 3D cell culture, and they can, so far, have not been used for drug screening based on cell metabolism [127-130]. In the two-dimensional cell monolayer, the biosensor was used to measure the metabolism of

hepatocytes in situ, and the commercial biosensor was combined with the microflow control platform to sample from the culture bottle [132]. However, in 2D, the total number of cells, medium volume and result concentration differ greatly from the 3D method. An optical sensor can be used to measure the dissolved oxygen well [133-136].

Sampling and jet transport are challenging because the oxygen supply in the atmosphere requires airtight fluid handling and analysis, which actually limits the way oxygen is measured in place. In cell culture, optical sensors are based on oxygen and pH, but multiparameter monitoring of other metabolites, such as lactic acid electrochemical sensors, is preferred. In 3d cell culture, the multi-tissue experiment of microstructure was realized by using the suspension network of microfluidic interconnection. They combine low volume, sphere constraints and medium exchange. However, the technical effort to manufacture and operate these devices is considerable, and open microfluidics requires precise and reliable liquid pumping equipment [137-139]. The enzyme, ampere lactic acid and glucose sensors are integrated on such suspension platforms. Short-term lactic acid production and glucose consumption in static conditions were measured from individual colon cancer cells to 1h. Setup requires a cyclic exchange medium that provides fresh media. More importantly, cells need to be stored in this particular system to obtain metabolic data. A microfluidic platform for three-dimensional cell aggregation has recently been demonstrated, including optical oxygen sensors and electrochemical glucose and lactic acid sensors. In this approach, commercial biosensors are placed in downstream microfluidic fluids [140-141]. This means can only measure the combined signal from multiple three-dimensional polymers, reducing the demand for highly sensitive sensors, because the concentration increased, but in the sample must be

exchanged in microfluidics. It also prohibits the aggregation of individual cells. Also demonstrated on this droplet platform is the electrical impedance measurement commonly used to adhere to 2D cell culture. Impedance mainly quantifies attachment to surface and/or mechanical integrity [142-145].

In three dimensional case, the applicability of the impedance is limited, because cell/tissue adhesion but always cover the whole volume, usually has a low number of cells or density, and is likely to have high heterogeneity. In addition, although the impedance does not allow the implementation of chemical sensors to measure metabolites. Traditional method measuring metabolites, such as taking sample or collected in the supernatant fluid, and then use the HPLC analysis or clinical analyzer, more easy to perform, but there are a number of shortcomings is that they only provide endpoint or snapshot information, at the same time, they don't allow online monitoring and analysis must be stable, they need to remove the media culture also need to be replaced, and parallelisation may not easy or labor-intensive industries [146-148].

Cell-based assays that can investigate cell biology, drug efficacy, metabolism and toxicology are dominated by technologies employing cells grown on flat plastic surfaces (2D) or in single cell suspension [149-150]. However, biology of cells is extensively influenced by the environmental context such as cell-cell contacts, cell-matrix interactions, cell polarity as well as the oxygen profiles (need reference).

Cancer researchers have recognized the biological characteristics of non-vascular tumors that have been detected and have been particularly well mimicked in three-dimensional (3D) cell cultures [151-153]. For example, one of the earliest effects associated with clinical observation in vivo is the development of multi-cell resistance

(MCR) in the development of anti-cancer drugs in 3D culture. Highlights Desoize Jardillier, cancer cells embedded in a 3 d environment on the anti-cancer drug sensitivity is low, as in the VLB exposed human lung cancer cell monolayer culture exhibition IC50 alue concentration of 0.006 (including mol/l, and sphere IC50 alue concentration of culture is almost 60 (including mol/l. More importantly, drug sensitivity is a net effect of a variety of factors, and is highly regulated by hypoxia conditions, which occur in the hypoxia region of the tumor and limited access to the capillary network [154-156]. Low oxygen pressure also leads to increased drug sensitivity or increased resistance to the tumor, depending on the mechanism and structure of the drug.

Additionally, the extracellular acidification is also another factor influencing response to either basic (such as Doxorubicin) or acidic (such as Choriambuses) drugs. In this case, the uptake of basic drugs is decreased, whereas the uptake of acidic drugs is increased, resulting in higher drug resistance or higher drug sensitivity, respectively [157]. Therefore, tumor cells cultured in 3D formats, which are exposed to a complex and heterogenic environmental context, there are more relevant tool to study tumor biology and responsiveness than standard 2D cell culture [158-159].

There are another example of cells with well documented influence of culturing conditions on physiology are hepatocytes cells [160-161]. Hepatocytes are characterized by their polygonal shape and multi-polarization with at least one basolateral and two apical surfaces. While the same time, the changes in cell form limit cell–cell and cell–matrix interactions, consequently can lead to reduced polarization, which can reduced bile canaliculi formation and a loss of important signaling pathways. Dedifferentiation of hepatocytes observed in 2D monolayer cell culture results in reduction of liver-specific

functions, such as the metabolic competence for detoxification, due to down-regulation of phase I and II enzymes. Therefore, maintenance of hepatocyte shape and function is of the utmost importance in hepatotoxicity studies [162].

Over the past decade, the central focus of drug discovery efforts has been in vitro models to better simulate the internal conditions of the target patients [163-164]. The initial step is to use the purification of drug targets, transfer from biochemical tests, support cell based approach, using excessive expression in normal host cell line drug targets, such as LN229 and Hela cell [165]. Correlation for more rapid response is the use of primary cells, if supply is adequate, it is best to humans, and depends on the expression of endogenous drug targets, detection technology should be sensitive enough. In these cell types, a large part of attachment is a natural, allow the cultivation of the simple workflow, in a plate was coated in cultured cells, and cultivation of micro board before [166], to encourage cell in two-dimensional (2D) monolayer cell adhesion. Although in biochemistry and immortal cell lines provides a preliminary improvement, but a lot of evidence to support such a reality, the cultured cells in 2D way is usually have a problem, and in the body condition and behavior is a model of a relatively poor [167]. Using a 2D model can reduce the rate of loss of cancer candidate drugs, which is about 95%, due to the non-conversion of the clinical drug efficacy value and the unanticipated toxicity problem. In last year alone, nearly 800 kinds of anticancer therapy in clinical trials and review of the federal drug administration (FDA), only 12 kinds approved, and led to in preclinical and clinical trials has spent hundreds of millions of dollars [168-170]. These defects can be traced back to the cause of the traditional two-dimensional condition, namely the extracellular matrix (ECM) components at the same time, the

interaction between cell and cell, the cell differentiation, proliferation and cell function is very important [171-173].

Although there are a lot of the same problem using 2 d cell culture to create accurate tumor model extended to liver toxicity studies [174], the gold standard of different biomass toxicity testing including in vivo animal experiment, improve the animal welfare issues, and the poor animal research results consistency in the heterogeneous population disease phenotype observation, integrating a feasible, it can predict priority [175] of the in vitro test method. Although for the liver cell line derived simplified, simplify the procedures, and eliminates the need for the whole animal experiment, but at the same time, participate in the first stage and second stage of metabolic gene expression spectrum with those observed in the liver tissue is not consistent. Primary hepatocyte culture provides a level of function that is closer to the body, but these cells are problematic when used in vitro. Under the traditional two-dimensional culture conditions, the cells dedifferentiate and rapidly reduce the expression of cytochrome P450 enzyme, eventually losing vitality [176-178]. Extensive studies have emphasized the limitations of two-dimensional cell culture, such as tumor and liver models in vivo, and emphasized the need for new cell models in research methods. This requirement can be met by the use of 3D cell models, because 3D cultured cells are more closely related to complex features in vivo [179-180]. Compared with the advantages of combining 3 d culture cell, 2 d cultural model, evaluation of drug candidates can include: (a) the oxygen and nutrient gradient, (b) increase the interaction between cells and the cell - to - the ECM, (c) non-uniform illumination test molecules in cells of the three-dimensional structure, different cell proliferation, (d) and (e) the influence of site specific

stromal cells in the tumor microenvironment. Studies have shown that when evaluated in 3D, tumor cells in specific cell lines are less sensitive to cancer drugs than they are when they are cultured in 2D. At the same time, however, other studies have shown that different cell lines, using different 3D technologies, exhibit the opposite effect [181]. These findings highlight, using 3 d cell culture in cancer research may provide key insights activity of drug in the body, if only in 2 d cell culture model as the research, may be neglected. In addition, the mechanisms that produce these differences can be clarified, such as changes in signaling pathways, or changes in the dependence of targets in three-dimensional systems, compared to cells cultured in 2D.

Table 1: The Advantage and Lamination of Four Types of Research

	2D cell culture	3D cell culture	Animal	Human
Advantage	➢ Cost effective ➢ Convenient for cell analysis ➢ High throughout screening feasible	➢ High Efficiency ➢ Low Cost	➢ Ensure the safety of therapy	➢ Provide accurate treatment information
Limitation	➢ An inaccurate prediction of in vivo	➢ More different environmental control	➢ Expensive ➢ Time-consuming	➢ Harmful ➢ Dangerous

2.2.2 Existing Methods for Generating 3D Microtissues.

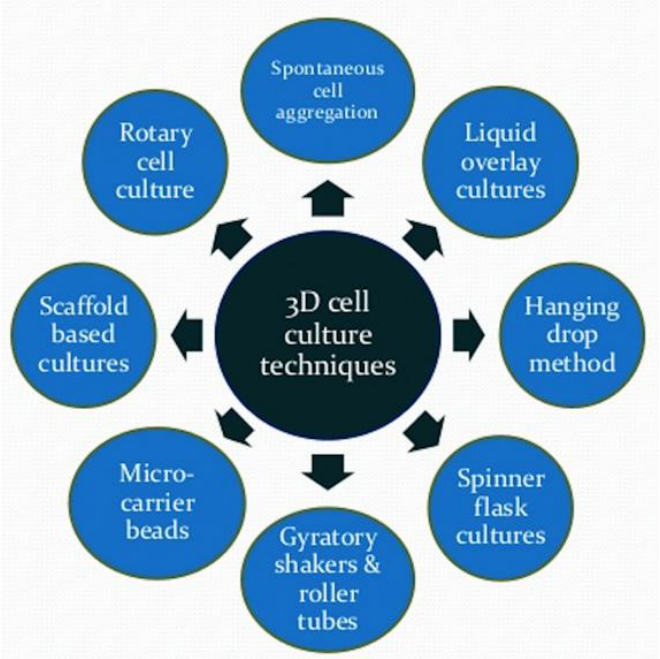

Figure 5: Existing methods for generating 3D microtissues.

2.2.2.1 Scaffold Based 3D Cell Culture

As we know, 3D tumors and other tissue models can be created by cultivating cells on prefabricated scaffolds that mimic ECM in the body. At the same time, the cell adhesion, migration, filling the gap in the stent, forming 3D culture [192]. Scaffolds are used as physical support systems for extracorporeal cell cultures and are also promising in tissue regeneration in vivo, as they are likely to reconstruct the natural physical and structural environment of living tissue. It has many common polymers of geometric configurations, including polystyrene (PS) and polycaprolactone (PCL).

Scaffolds can also be made from more natural or biogenic components, such as proteins that are common in ECM. These usually include, but are not limited to, fibrin,

collagen, laminin, and gelatin. Biological scaffold provides not only the cells of a matrix can be attached and restructuring into three-dimensional structure, but more importantly, they provide the correct microenvironment of soluble growth factors, hormones, and other molecules, cells in the body environment interaction, so as to change the gene and protein expression. The current approach requires that the cell before electroplating, in a liquid state (collagen) mixed with scaffolding protein, or on the scaffold for the formation of before sowing, or will have been aggregated into three-dimensional sphere of protein mixture covering on the cells. Cells can then be reorganized into the surrounding environment, releasing signal molecules, allowing migration, or regulating other cellular functions. The final result is an appropriate steady state. 3D cell culture method is widely seen as better than the traditional 2D cell culture method of physiology significance, and can in the early stages of drug development process to improve drug candidate [193].

The visualization of 3D structures is challenging problem, such as when imaging microtissues there is slightly scattering and absorption which prevents imaging deep into the center of the microtissue. Here, we show how the boundaries of microtissue imaging can be pushed further by using the Opera High Content Screening System (equipped with a water objective lens) in combination with a microtissue pretreatment. The aqueous reagent (Scale) renders the biological sample optically more transparent and allows a greater imaging depth. It also describes the analysis of a spherical colon cancer microtissue model using in vivo near infrared (NIR) agents. These agents allowed visualization and quantification of cancer-associated biomarker intensities and their distribution in microtissues. It can be also detected that the expression of these biomarkers and the observed oxygen gradients correlate with the development of solid

tumors in vivo, confirming microtissues to be a physiological cell model suitable for cell-based drug screening at the same time [194].

2.2.2.2 Non-Scaffold Based 3D Cell Culture

After a long incubation of cell spheres and toxicity tests, cell globules are usually transferred from suspended drop plates to another petri dish that can accommodate larger media or buffer volumes [195]. Larger volumes can ensure that the aggregated cells are in the right conditions, such as nutrient levels, pH values, and reproductive cycles for days or even weeks. The hanging drop plate (HDP) USES the fact that cells assemble themselves into a three-dimensional cluster structure without the surface attached. Each plate meets the SBS standard, but at the bottom of the HDP well contains an opening, compared with the normal well at the bottom. HDP Wells at the top of the similar traditional microplate cells can distribute in the media, at the bottom of the hole carefully designed to form a discrete droplet media meet cell aggregation, in contrast, but also small enough, the surface tension can be off to prevent water droplets in the manipulation. The cells in the suspended medium gather together within hours to form the final spherical structure. The size of the cell cluster is controlled by the number of cells. The co-cultured spheres can also be created by adding multiple cell types at the initial allocation, or in order, allowing each group of cells to be aggregated into different layers [196].

Using three-dimensional microstructure as the intermediate model between two-dimensional cell culture and animal model, radiation induced cell and DNA damage was assessed in the background of personalized radiotherapy. An agarose gel microwave array is used to generate three-dimensional microstructures with control dimensions and

shapes. These microstructures are exposed to different doses of X-ray radiation and use different endpoint techniques to detect radiation damage to cells. The cell membrane damage and metabolic activity were decreased by MTT assay, and staining was carried out. DNA damage and micronucleus analysis test, gamma –H_2AX verruca, and HaloChip assay. Exposed to X-ray 3D microstructure and the extension of culture in the unexposed microstructure compared to smaller, this shows that the X-ray radiation can slow the growth of micro three-dimensional tissue cells, cell outer cells can prevent further injury of the cells [197-198].

The radiation sensitivity of different tumor types and patients with different types of tumor was very different. One important requirement is to predict the efficacy of radiotherapy for individual patients. Radiotherapy in the treatment of choice for a particular patient is by the clinical and pathologic features of the tumor, and the objective is to identify patients with individualized radiotherapy for radiation sensitive, from radiation therapy in low-risk patients may receive additional benefits, and high risk for surgery. At the same time, this personalized approach can provide patients with an alternative dose plan to reduce the total radiation dose. The radiosensitivity of the tumor can be evaluated by the systematic biological method. Biomarkers extracted from tumors can also be used to predict radiation sensitivity, but the predicted results are heterogeneous due to epigenetic control gene expression [199].

As mentioned above, 3D cell culture technology is dedicated to rebuilding the three-dimensional structure of tissues and tumors in vivo, as well as the interaction between cells and ECM. The microfluidic platform can also be used to create a similar heterogeneous model and increase the complexity by introducing an infiltration flow to

the cell environment. Allows continuous nutrition and oxygen imports, as well as the removal of waste through the medium. At the same time, cells are maintained in a compartment through different physical or non-physical barriers. The medium contains nutrients, chemicals, molecules or staining reagents, which are then infused into the cells. The spacing between the preset obstacles allows the compartment to interact with each other [200].

In addition to the geometry differences, ECM almost can regulate cell function (such as migration and toxic effects), cell mechanics, such as the stiffness and the cell - matrix adhesion), diffusion characteristics (such as drugs, oxygen and free radicals), and the ability to repair damage caused by external stimuli such as ionizing radiation and environmental toxins. Three-dimensional (3D) aggregation of cells can simulate the structure and function of human body in the environment near physiological conditions. At the same time, the stability of these cells was higher than that of the 2D medium. Cell function has good a major role in tissue culture, compared with 2D train, the three dimensional micro organization of cells may have enhanced ability to repair or damage tolerance, and surface area of the three-dimensional microstructures is less than 2D cell monolayer cells. It is believed that the toxicity test of 3D tumor microstructure can fill the knowledge gap between 2D cell detection and living animal experiment in vitro [201-202].

Add physical barriers are usually in microfluidic device is composed of glass or silicon, including polydimethylsiloxane (PDMS), polymathic methacrylate (PMMA), polycarbonate (PC) and polystyrene (PS), in addition to chromatography or filter paper. Cells can also be combined with a supportive substrate, such as collagen or matrix, to

encourage cell ecm interaction and encourage the assembly of three-dimensional structures. The introduction of ECM also allows the creation of microfluidic devices that do not contain physical barriers. Matrix polymerization maintains cells in pre-defined cultural areas and also ACTS as a filter during the flow. Microfluidic systems are also used in various 3D cell culture applications, including stem cells, primary and cancer cells. Yu et al. developed a three-dimensional microfluidics cell culture system and applied the system to the study of the extracorporeal differentiation of BMSCs in rats (ref.). Wan et al. also developed PDMS devices to study the differentiation of mouse embryonic stem cells into cardiomyocytes (ref). Finally, Liu, et al., combined with a microfluidic device, studied the role of cancer-associated fibroblasts in the invasion of tumor cells [203].

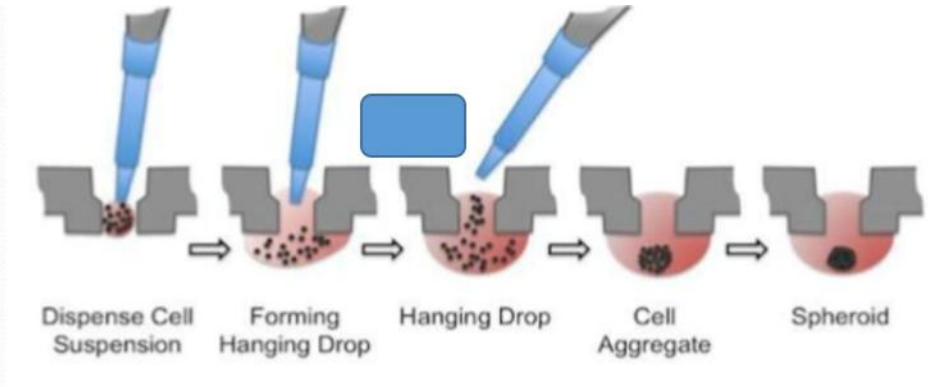

Figure 6: Hanging drop techniques.

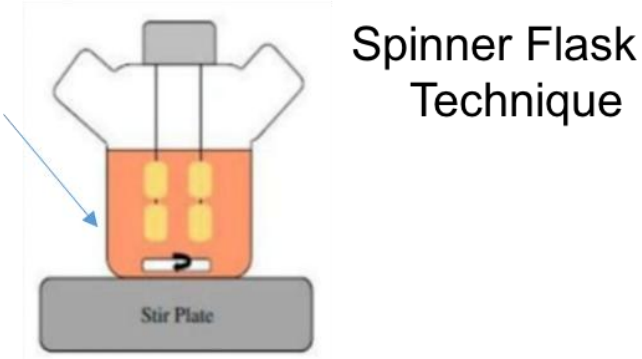

Figure 7: Spinner flask technique.

2.3 X-ray Irradiation on 3D Microtissues

2.3.1 X-ray Generation

It was discovered by physicist W in 1895. Roentgen, x-rays are widely used for diagnosis and treatment. X-rays have high penetrability and invisible electromagnetic radiation that can produce images of tissues, bones and organs, and can detect tumors inside the body. X-rays are much more likely to be absorbed by bone than the surrounding blood and tissues, and these images can be compared to identify solid tumors or lesions. In addition, the cells and tissues of X-ray irradiation can produce free radicals, which damage the DNA in tumor cells, as described in section 1.5 using X-ray, can simultaneously detect and treat cancer. X-rays are usually generated by a potential difference that accelerates electrons and directs them to the target material (usually tungsten). High-energy electrons decelerate in the strong electromagnetic field of the electron or nucleus of the target atom. At the same time, the deceleration of fast moving

electrons produces a continuous spectrum or brake radiation and characteristic X-ray of bremsstrahlung. The continuous spectrum of the braking radiation extends from zero to the initial energy of the particle. For the peak of the characteristic X-ray, their energy corresponds to the energy level of the atomic electron in the target. In continuous bremsstrahlung radiation x - ray spectrum superposition characteristic x – ray[204].

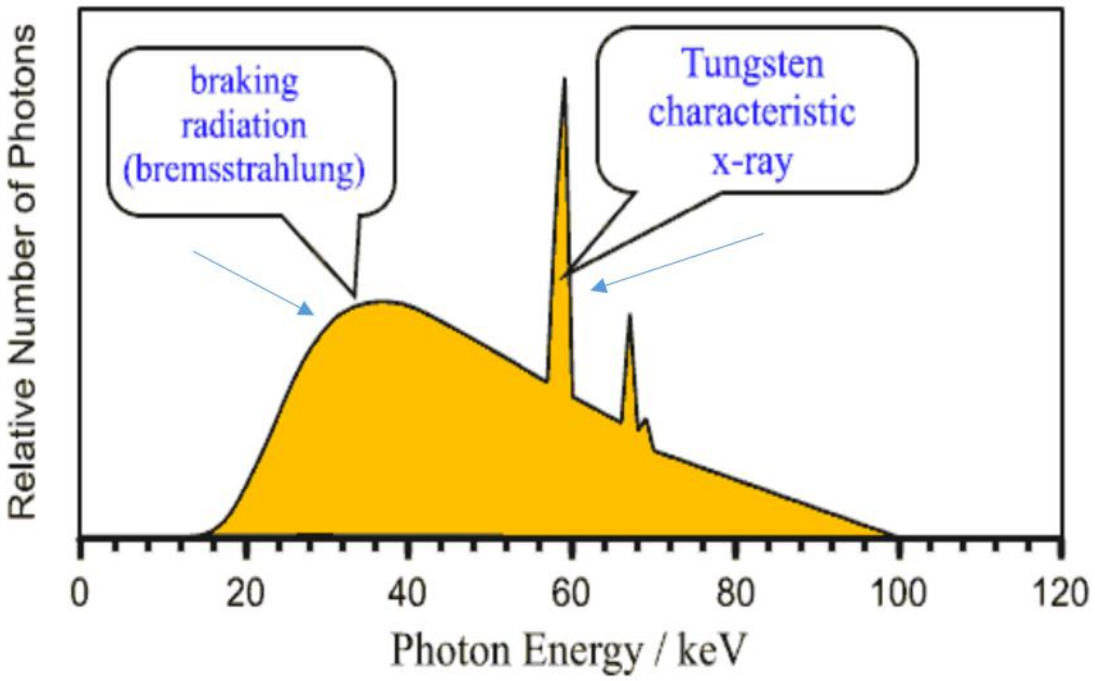

Figure 8: X-ray spectrum from a tungsten X-ray tube.

2.3.2 X-ray-Matter Interaction

Figure 9 shows the various methods of interaction between x rays and materials [119]. It shows the original, unattenuated radiation that does not interact with each other. The main interactions between the diagnosis and treatment of x rays include elastic and inelastic scattering and photoelectric absorption. There is no discussion of the pairing of extremely high energy (1.02 MeV) X-ray

photons.

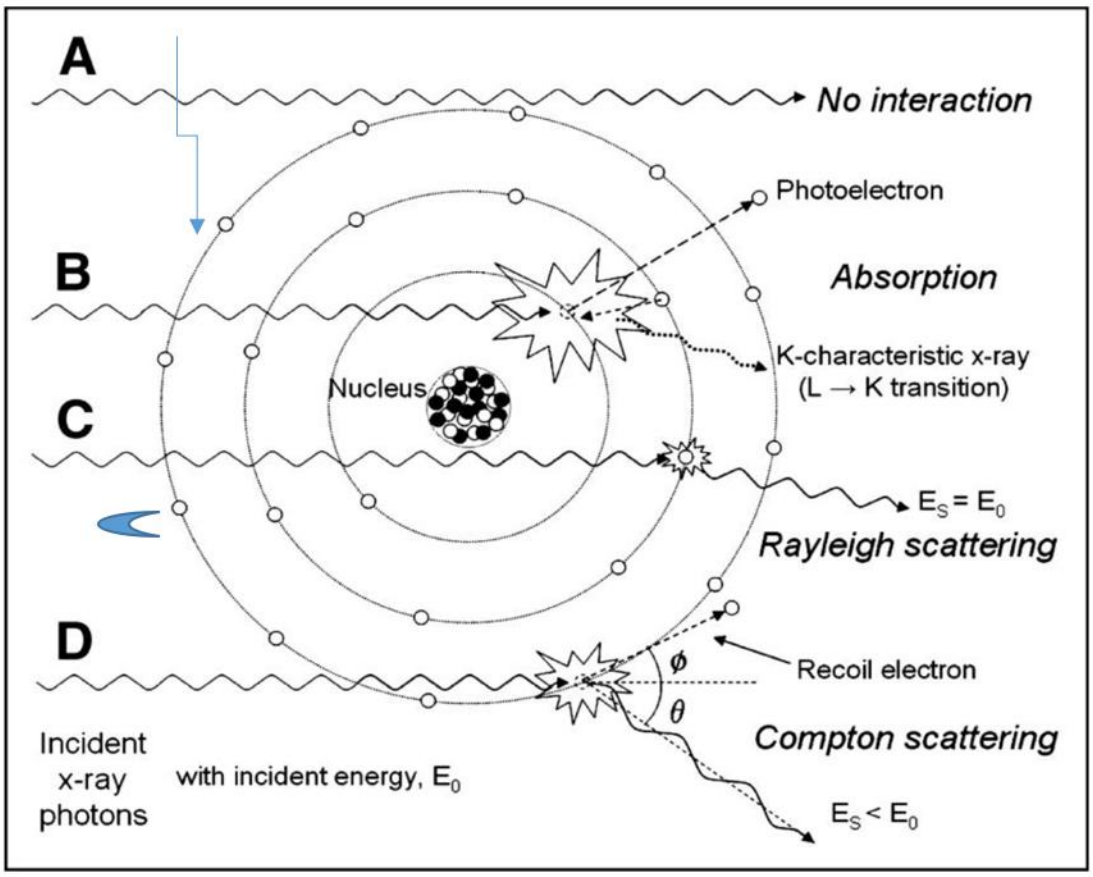
A
No interaction
Photoelectron
B
Absorption
K-characteristic x-ray
(L → K transition)
Nucleus
C
$E_S = E_0$
Rayleigh scattering
D
Recoil electron
ϕ
θ
Compton scattering
Incident
x-ray
photons
with incident energy, E_0
$E_S < E_0$

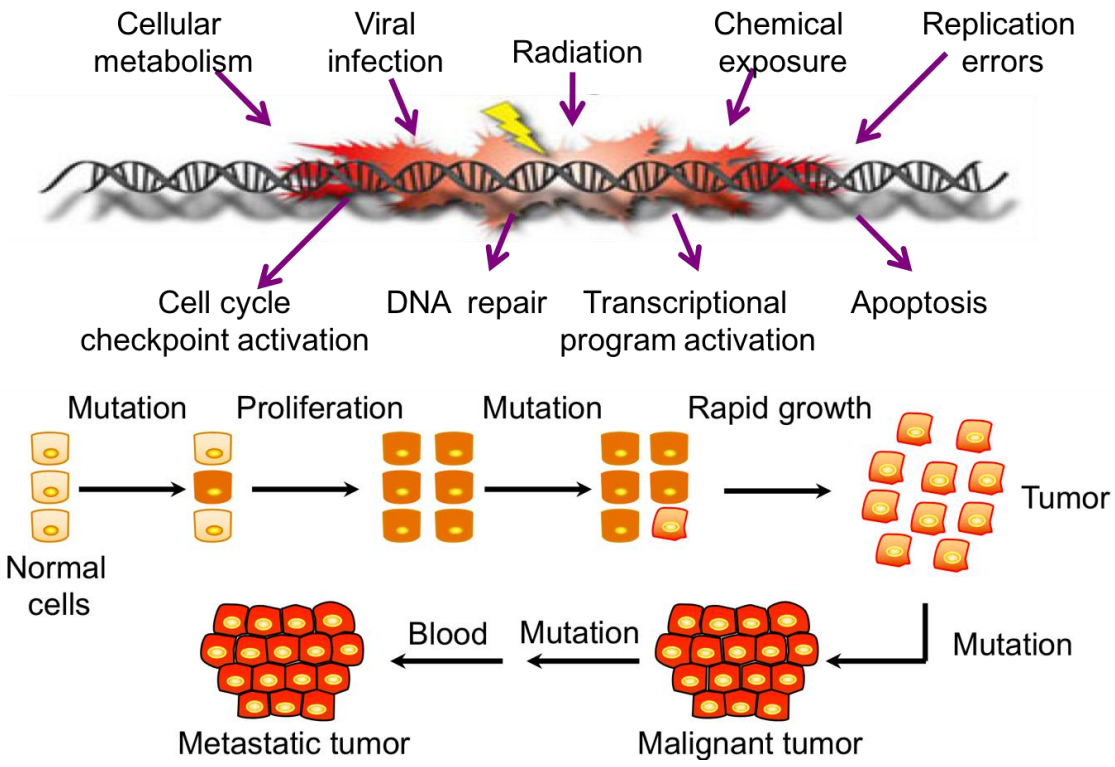

Figure 9: X-ray interactions with atoms.

In elastic or Rayleigh scattering, an incoming X-ray photon collides with an electron in an atom. In a collision, the incident X-ray photon has no energy loss (as shown in the figure). The energy of the electron has been increased, but it has not been removed from the atom. When the electron goes back to its previous energy level, the X-ray photon energy released by it is equal to the energy of event 1, but in a slightly different direction. The probability of Rayleigh scattering increases with the increase of the target atom Z, and the X-ray energy decreases [205].

Currently, chemotherapy, surgery and radiotherapy are the most aggressive treatments for cancer. Radiation therapy targets and destroys tumors by ionizing radiation. The laser produces free radicals that destroy all kinds of cellular components, including DNA. One of the advantages of using radiation therapy is that it kills tumors, even if they

are mixed with normal healthy tissue. As a result, more than 50% of cancer patients received radiotherapy. However, the therapeutic dose used in radiotherapy can damage nearby normal cells. Various chemicals and nanoparticles are tested as radiosensitizers to enhance radiation therapy [206-207].

Although cell membranes play an important role in maintaining cell function, cell membranes are the major barrier to the delivery of nanoparticles. So even if ion or nanoparticles plateau z elements (such as gold, platinum and bismuth) was used to improve the radiation therapy by ionizing radiation absorption and generates free radicals in high yield and to enhance the measurement, such as the e has negligible because of the nanoparticles, may be because the happy letters coefficient of nanoparticles in cancer cells and X-ray produce free radicals is unable to be near the DNA damage. For inelastic or Compton scattering, the energy Eo's X-ray photon is larger than the binding energy of the atomic electron, colliding with the electron in the atom. The photon passes all or part of the energy to the electron. The electrons that receive some of the energy from the X-ray photon recoil from the atomic point of view. The rest of the energy Es is transferred to the scattered X-ray photon deflection Angle of theta and relative to the incident photon. The probability of Compton interaction is proportional to the electron density of the relevant material and is independent of the energy between 10 and 150kev. At 150kev, the probability is approximately 1/ Eo [208].

The probability of photoelectric absorption is proportional to the cube of the atomic number of interacting atoms, which is inversely proportional to the cube of energy, such as Z3/Eo3. When an incident X-ray photon has enough energy to emit an electron from the atom, this phenomenon is described as photoelectric absorption. The kinetic

energy of the emitted electron is given by the difference in the binding energy of the incident X-ray photon energy Eo and the electron shell. The photoelectric interaction is more likely to occur when the atomic number is higher and the X-ray energy is lower. In the photoelectric effect, at the same time, the ejection from shell electronic leave atomic excited state soon return to its steady state through the two possible mechanisms: this is X-ray fluorescence and auger effect, and the first effect caused by the discharge characteristic x ray another electronic ejection which results from the atom (auger electron) [209-210].

3.0 Experiments

3.1 Materials

The kits for Vybrant MTT cell proliferation, Vybrant cytotoxicity, live/dead assays, and Quant-iT PicoGreen dsDNA assay were from Invitrogen (Carlsbad, CA). NaBH4, RPMI 1640 culture medium, penicillin, streptomycin, fetal bovine serum (FBS), and Dulbecco's phosphate-buffered saline (D-PBS) were from Sigma−Aldrich (St. Louis, MO). Anhydrous dimethyl sulfoxide (DMSO), toluene, poly (vinylpyrrolidone) (PVP), 3-aminopropyltriethoxysilane (APTES), ironoleate, tetraethyl orthosilicate (TEOS), octadecene, diphenyl ether, sodium oleate, and methacrylic acid (MAA) were from VWR (West Chester, PA). Ultrapure water from Nanopure System (Barnstead, Kirkland, WA), Synergy HT multimode microplate reader from Biotek (Winooski, VT) was used for absorbance and fluorescence measurements. HeLa (CLL-2) and MG-63 (CRL-1427) cell lines were from American Type Culture Collection (ATCC, Manassas, VA). Inverted optical micros- copy from Milesco scientific (Accu-Scope 3032, Princeton, MN) was used to observe cultured cells. Fluorescence images of microtissue were taken on a Zeiss Axioskop 2 mot plus confocal microscope and an inverted fluorescence microscope from Olympus (GX51). All chemicals used in this study were analytical-grade and were used without further purification.

3.2 3D Microtissues Generation

3.2.1 Cell Culture

HeLa and MG-63 cell lines were used to study three-dimensional microstructures and 2D single-layer cells. 3 d microtissue culture is as follows :50 mu L 2% of agarose

gel was introduced to each good by 96 - microplate. The microplate wobbles gently and spreads the gel evenly over the bottom, and any bubbles are removed. After 10 minutes, a solid non-viscose agarose gel was formed in each well of the microplate. All hela and mg-63 cells were grown in RPMI 1640 to supplement penicillin (100 units/ml), streptomycin (100 mg/ml), and 10% fetal bovine serum full-backs. HeLa and mg-63 cells were cultured under the ATCC protocol., in a nutshell, the 20 cell suspension in each well into a final concentration of 1/105 of cells/mL, then put the cell culture in an incubator, 5% of the CO2 in an incubator, at 37 degrees Celsius under 12 hours of training, make the 3 d tissue formation. These cells tend to aggregate and form a circular microstructure on the surface of the non-viscose gel [211].

3.2.2 3D Micro-mold Generation

A 2% low melting point of agarose (85 C) is melted and poured onto a tray, where the micropores are placed at the top until the agarose is solidified. The American Type Cell Culture (Manassas, VA) was cultured in the 2D Cell Culture dish, and cultured in the RPMI 1640 Culture dish for 1-2 days until it reached 80% of the confluence. Using 0.25% trephined, separation of cells after 1000 RPM centrifugal hemocytometer determination for 5 minutes, and then sow 2 x105 cells in culture, in 9 x9 array of microwave, about 2.4 x 103 cells can occupy a very well. The use of agarose as a matrix minimizes the interaction of the substrate, and the adhesion between cells can spontaneously assemble the cells into three-dimensional microstructures within an hour.

3.3 X-ray Exposure

A Mini-X X-ray tube (Amptek, Inc., Bedford, MA) operating at tube voltage of 40 kV and current of 100 μA is used to generate primary X-rays. Mini-X X ray tube (Amptek Inc.), Bedford,MA) operates tube voltages 100 kV and the current one is mainly used to generate X rays. The surface dose rate, 5 cm from the tube, was measured with the hand-held radiation dosimeter (Mirion rad-60, freshwater system, Greenville, SC), and was found to be 0.4gy /h. In the 99th group (~ 1d), microwellsthe cell was fixed in a distance of 5 centimetres, which is a new kind of new beam. The X-ray beam covers the exposed surface of the ~2.4 cm2 region and is sufficient to evenly illuminate the entire array. In the X-ray irradiation time and different from 1 min to 1 h, trypan blue, a kind of fluorescent dye, a blue tint to dead cells, at the same time don't change the living cells, add it to the microwave, staining cells in the micro organization. By introducing three cell lines (HeLa, mg-63) into a single biological dosimeter, high-throughput radiation detection and monitoring can be achieved. By means of the control of liquid 1, the cell suspension was used for each microwell to use the volume tip, and different Microsystems used the same array biodosimeter high throughput application.

3.4 Cell Culture with Gold Modified Nanoparticles

HeLa (CLL-2) and human fibroblasts (CCL-110) cell lines were obtained from the American Type Culture Collection (ATCC). Cells were cultured in a tissue culture flask (Thermo Scientific, Cambridge, MA) in an incubator at 37°C in an atmosphere of 5% CO_2 with DMEM medium (BioWhittaker, Walkersvile, MD) that is supplemented with 10% serum, 1% penicillin-streptomycin (Sigma-Aldrich, St. Louis, MO) and 2 mM glutamine (Life Technologies, Cambridge, MA). Cells were seeded in a 96-well

microplate at a concentration of 5,000 cells per well. After 24 hours, CPP modified gold nanoparticles were incubated with cells at a final concentration of 2, 10, 20, 50 and 100 μM, respectively. Excess nanoparticles in the medium were removed after incubation for 24 hours. Cells grown in 75 cm^2 culture flasks with respective concentrations of nanoparticles were imaged at 24, 48 and 72 hours with or without X-ray using a IX71 Olympus microscope and Hamamatsu digital camera. A Mini-X portable X-ray tube (Amptek, Bedford, MA) with a silver anode operating at 40 kV and 100 mA is used to generate primary X-rays and irradiate cells at a distance of 5 cm for 15 minutes for all X-ray irradiation experiments.

3.5 Cellular Damage Detection

3.5.1 Cell Viability

G6PD (glucose-6-phosphate dehy-drogenase), calcein AM/EthD-1 (calcein AM and ethidium homodimer), and MTT [3-(4,5-dimethylthiazol-2-yl)-2,5-di-phenyltetrazolium bromide] assays were done by following the standard protocol from suppliers. The G6PD(glucose-6-phosphate dehydrogenase), calcein AM/ ethd-1 (calcein AM and ethidium homodimer), MTT[3-(4, 5-dimethylthiazol-2-yl)-2, 5-di-diphenyltetrazolamine]assays is carried out in accordance with the supplier's standard protocol. For MTT assay, the culture medium in each well was removed and replaced with 100 fresh medium. The solution for 10ml of 12mm MTT stock is to add to each good, to a negative control medium (100 for no nanoparticles). After the incubation, 37th C 4 h,100 L SDS - HCl solution was added to each solution by removing liquid and mixing thoroughly. 37 ° C for 6 h after hatching, mixing and each sample tube and optical absorption 570 nm was recorded. For G6PD detection, 50 L(2) resazurin/ reaction

mixtures were added to each well, as well as live and fully dissolved control cells. The cells were added to the 1 cell to dissolve the L 100 x cell lysis buffer. All the samples were tested in six copies. The microplate was incubated in 37 C for 30 minutes, and the fluorescence intensity was measured at 580 nm at 550nm. The background fluorescence was measured by the method of no cell control and was subtracted before calculation. The percentage of living cells and dead cells is calculated according to the equation provided by the donor. Cell viability was monitored in real time, including HeLa, mg-63 cells. This is done by measuring the color intensity of the image taken every 30 minutes after an X-ray (0.4gy). Image Pro Plus 6.0 (Media Cybernetics, Bethesda, MD) was used to analyze the Image, which could correct the background and obtain the color intensity of the area of interest. In addition, MTT assay was performed on 3 cell lines at 30 minutes after exposure to 0.4gy x rays. MTT assay can measure cell membrane integrity to detect living cells or dead cells.

3.5.2 Live/Dead Assay

Calcein AM/EthD-1 (calcein AM and ethidium homodimer), and MTT [3-(4,5-dimethylthiazol-2-yl)-2,5-diphenyltetrazolium bromide] assays were done by following the standard protocol from suppliers. For calcein AM/EthD-1 assay, 100 μL of D-PBS was added in each well to wash cells to dilute serum-containing esterase. Then 100 μL of dual- fluorescence calcein AM/EthD-1 assay reagent was added into each well, and the plate was incubated for 30 mins at room temperature before fluorescence intensity was measured. A cell free control was used to measure background fluorescence, which was subtracted before calculation. The percentages of live and dead cells were calculated by the equation provide by the supplier.

3.5.3 Cell Apoptosis Assay

Cell apoptosis in the presence of X-ray radiation was examined with annexin V-FITC/PI kit (BD Biosciences, Cambridge, MA) was used flow cytometry. Annexin V conjugated with fluorescein isothiocyante (FITC) labels phosphatidylserine sites on membrane surface, and propidium iodide (PI) differentiates apoptotic cells from viable and necrotic cells. In normal viable cells, phosphatidylserine (PS) is located on the cytoplasmic surface of the cell membrane. However, in the intermediate stages of apoptosis, PS is translocated from the inner to the outer leaflet of the membrane, exposing PS to the external cellular environment where it can be detected. Highly fluorescent annexin V conjugates provide quick and reliable detection methods for studying the externalization of phosphatidylserine. 10^5 cells were seeded in flat-bottom 96-well microplate to form three dimensional microtissue, X-ray irradiated microtissues was re-dispersed into isolated cells by treating the microtissues with trypsin and pipetted up and down. After being washed twice with phosphate-buffered saline (PBS), cells were gently re-suspended in annexin-V binding buffer and incubated with annexin V-FITC/PI in dark for 15 min. The extent of apoptosis was determined by using a Becton-Dickinson FACScan cytoflurometer (Mansfield). The fraction of cell population in different quadrants was checked by quadrant statistics.

3.5.4 Micronucleus Assay

The cells in the microtissues were re-dispersed into isolated cells, cytochalasin-B was added, and incubated at 37°C in 5% CO_2 for 24 h. The cells were then fixed with 4% para-formaldehyde in PBS for 10 minutes and treated with 0.1% Triton X-100 in PBS for 5 minutes. Cell nuclei were stained with DAPI.

3.6 Genomic Damage Detection in 3D Microtissues

3.6.1 Immunofluorescence Assay

Immunostaining of X-ray irradiated cells was performed as follows. The x - ray irradiation cells were stained with immunity. The cells were cultured on the cover glass 6 well plates and exposed to x rays (100 kV, g A) for 15 minutes. Day after irradiation, cells were 4% paraformaldehyde fixed 10 minutes, wash with washing buffer 3 times, at room temperature in the block buffer (1% BSA, and 0.2% of Triton - 100 X) in PBS training 3 times. Main antibodies of anti - vinculin - FITC (sigma, 1:2000), add and incubated overnight at 4 ° C block buffer. The next day, three times were washed in the wash buffer, and two hours of rabbit secondary antibodies were added at room temperature (in vitrogen, 1:200). The cover has been washed three times before installation on the glass slide. A laser confocal microscope (Zeiss) was used to collect all images with a magnification of 80 magnification. The cells attached to the multilayer array were embedded with agarose gel (0.1% mass ratio); After the gel solidified, the slide was incubated with 0.3 M sodium hydroxide for 10 minutes at room temperature, with 10 g/ml SYBR 10 minutes. The drop in deionized water is the removal of the redundant BYBR fluorescence observation 3 minutes before hatching. The evaluation of micronuclear expression is as follows: X-ray irradiation microstructure redistributes the trypsin to individual cells and moves up and down. Cell division B (5 g/ml) was added to the cell culture medium. The cells were cultured for 24 hours prior to 37-c and 5% of co2 trypsin. In PBS, the cells were fixed for 15 minutes with paraformaldehyde, and PBS

treated lysis with 0.1% Triton x-100. The cell nucleus was staining with DAPI (0.2 g/ml, 15 min) and imaging under a fluorescence microscope.

To assess the expression of DNA repair protein (γ-H_2XA), X-ray irradiated microtissues was re-dispersed into isolated cells by treating the microtissues with trypsin and pipetted up and down. The cells were cultured at 37°C and 5% CO_2 for 30 min, fixed with 4% paraformaldehyde in PBS for 10 min, and treated with 0.1% Triton X-100 in PBS for 5 min. After incubating in blocking buffer (3% bovine serum albumin in PBS) for 1 h, primary antibody against γ-H_2XA was added and incubated at room temperature for 2 h. After rinsing with PBS, cells were incubated with FITC-washed with PBS. Nucleus of the cells were stained with DAPI (0.2 μg/mL) for 15 min, washed with PBS and observed under fluorescence microscope.

Cell viability test was performed by treating microtissues with X-ray every 2 days. During each treatment, microtissues were treated with X-ray for 3 mins and 15 mins. This step was repeated to three different area of microtissues so as to cover most cells in microtissues with enhanced radiation. Phase contrast and fluorescence images of cells were taken with Olympus IX 81 or Carl Zeiss (VivaTome) optical microscopes.

3.6.2 Cell Array Formation

After radiation for the microtissues in agarose mold were then put back to 5% CO_2 at 37°C. Then, when the microstructure was irradiated in the agarose model, it was reduced to 5 percent of CO2 at 37 degrees centigrade. The DNA damage in cells was evaluated by HaloChip analysis, micronucleus test and DNA repair protein expression. To conduct the HaloChip experiment, the microstructure of the X-ray irradiation was treated with trypsin for 5 minutes and transplanted into the isolated cells. A PDMS

imprinted microcolumn array was prepared with PSS, PSS, PAH-RITC and other polyelectrolytes as carriers. The stamp is printed on a glass substrate to form an isolated polyelectrolyte array. The cells in the medium are incubated on a glass substrate and the cells are attached to a polyelectrolyte array by electrostatic action. The unattached cells were rinsed with PBS.

3.6.3 Reactive Oxygen Species (ROS) Production

Carboxy-H2DCFDA was used to measure ROS production from X-ray irradiation. In the presence of ROS, carboxy-H2DCFDA was oxidized and emitted green fluorescence. Carboxy-H2DCFDA was added at a final concentration of 1 μM into the wells of 96 well microplates. Gold nanoparticles were added at a concentration of 2, 10, 20, 50 and 100 μM a day prior to the experiment. The microplates were incubated in the dark for 30 minutes. The medium containing carboxy-H2DCFDA was removed and cells were washed twice with phosphate-buffered saline (PBS). After adding fresh medium, cells were immediately irradiated with an X-ray (40 kV, 100 μA) for 15 minutes, followed by incubation for one hour. The fluorescence intensity was measured using a fluorescence plate reader using 492 nm excitation and 527 nm emission wavelengths, respectively. Two independent experiment sets were performed. The distribution of ROS after X-ray irradiation was imaged as follows: the cells were cultured in coverslips, exposed to X-ray radiation, treated for the ROS experiments, fixed by 4% paraformaldehyde for 10 minutes, washed with PBS, and mounted onto glass slides.

Two independent experiment sets were performed. e distribution of ROS a er X-ray irradiation was imaged as follows: the cells were cultured in coverslips, exposed to

X-ray radiation, treated with reagent, red by 4% paraformaldehyde for 10 minutes, washed with PBS, and mounted onto glass slides.

3.6.4 DNA Damage Observation

A day after cells were incubated with gold nanoparticles in a 25 cm^2 tissue culture flask, cells were exposed to an X-ray (40 kV, 100 μA) for 15 minutes, trypsinized after 24 hours, and re-plated onto a 6 well culture dish with sterilized coverslips at the bottom of each well. Once cells attached to coverslips, cells were mounted on a glass slide using mounting medium vetashield (Vector) containing DAPI (4',6-diamidino-2-phenylindole). DAPI is a fluorophore that can be used to visualize nuclei content by binding strongly to adenine-thymine rich regions in DNA. If there was any serious DNA damage, the change in nuclei morphology would be observed through DAPI staining. The samples were visualized using a confocal microscope (ZEISS), and more than 60 cells were counted to determine if their DNA was damaged. Ionizing X-ray radiation causes water radiolysis, generating intra-cellular reactive oxygen species (ROS). ROS can cause oxidation damage to DNA, resulting in single or double DNA strand breakage and giving rise to genomic instability. To determine if PEG-CPP modi ed gold nanoparticles can enhance ROS production a er X-ray irradiation (40 kV, 100 mA), HeLa cells were incubated overnight with various modi ed gold nanoparticles. An 11 fold increase in ROS production was observed exposed to X-ray radiation, as compared to untreated cells.

3.6.5 Double strand break

The expression of the DNA repair protein (γ-H2XA) was deter- mined to assess DNA double strand break as follows. Microtissues were re-dispersed into discrete cells by

using trypsin and pipetting up and down. The cells were cultured at 37 °C and 5% CO_2 for 30 min, fixed with 4% paraformaldehyde in PBS for 10 min, and treated with 0.1% Triton X-100 in PBS for 5 min. After incubating in blocking buffer (3% bovine serum albumin in PBS) for 1 h, the primary antibody against γ-H2XA was added and incubated at room temperature for 2 h. After rinsing with PBS, the cells were incubated with FITC-

washed with PBS. Nuclei of cells were stained with DAPI (0.2 μg mL^{-1}) for 15 min, washed with PBS and observed under a fluorescence microscope.

3.7 Detecting 3D Microtissue Migration

3.7.1 Detecting 3D Microtissue Migration Dependence on Matrigel Density

Flasks of cells were stained with a live cell membrane dye CMFDA (Molecular Probes), washed twice with calcium and magnesium-free Dulbecco's PBS, and resuspended in 1 ml of phenol red-free DMEM. Using the active cell membrane dye CMFDA(molecular probe) staining, washing twice with the PBS wash of calcium and unmagnesium Dulbecco, and refloating in 1ml of phenol red free DMEM. Using the active cell membrane dye CMFDA(molecular probe) staining, wash twice the calcium and the UN magnesium Dulbecco with PBS, and refloat in 1ml of phenol red free DMEM. Cell suspension (50 L) combined with serum DMEM, substrate (final concentration of 50 to 200 L final volume). The matrix also contains 1-m sulfate fluorospheres (molecular probes), which can be detected at 580/605 nm as a signal for evaluating matrix movement.

After 1h, the matrix was covered with 2 ml phenol red - free DMEM and 5 h incubation. The cells were magnified 25 times with the PerkinElmer rs-3 confocal microscope (499 nm). In six hours and the lower part of the collection of a series of time-lapse images, each image by 100 m z - stack 0.5 m interval segmentation, image further analysis in each sample and using Matlab software to measure distance. Viability and form. After 24 hours, according to the manufacturer's agreement, A and AC live dead cell staining kit (Korean biological vision, South Korea) staining according to the manufacturer's agreement. After washing with PBS, fix it in a formaldehyde solution and embed it in the best cutting temperature (O.C.T.) compound (SAKURA tissue-tek, USA) for 12 hours and then freeze. The frozen cluster is divided into 10 micron thick samples - 20 C and slides. In the concentration of 2, 4 and 6 mg/mL, the 3d microstructure was prepared with rat tail collagen and fixed in the formaldehyde solution. The fixed gel is then embedded in the compound for 12 hours and then frozen. The samples of the frozen gel were divided into 10 mu and m thick part - 20 C, and attached to the glass slide. Cluster behavior in collagen gel can be used to monitor Axio observer microscopy (German Zeiss) incubation 0,6,12,24,48 h. Cluster formation, hela cells (PKH67 green fluorescent cells linker mini tool, sigma, USA) and hela cells (PKH26 red fluorescent cells linker mini tool, sigma, USA) were seeded in 96 - PS plate coating growing medium. In each collagen gel concentration and latency, cell migration is defined as the distance from the cell center to the image J software.

3.7.2 Scanning Electron Microscopy (SEM)

On the basis of this, a scanning electron microscope image was obtained. After washing with PBS, the 2.5% glutaraldehyde solution was fixed in 4 C for 30 min, and the fixed

cluster was maintained in 2% osmium 4 oxides (OSO4), 2 hours for 2 hours, and deionized water was used for cleaning. After the diluted ethanol was dehydrated, the hexamethylsilicate (HMDS) was vaporized and then stored in the vacuum chamber for one day for imaging experiments. The SEM image was then obtained using the s4100.

3.7.3 The morphological changes of clusters

Cells were fixed by 4% paraformaldehyde for 10 min, washed with 0.2% Triton-X 100 in PBS for 3 times and incubated at room temperature in PBS containing 1% BSA, and 0.2% Triton-X 100 for 1 hr. Primary antibodies for anti-vinculin-FITC antibody were incubated overnight in a blocking buffer at 4°C. After washing coverslip in the next day, rabbit secondary antibody was added in and incubated for 2 hr at room temperature. After washing cover slip, cells were checked with a laser confocal microscope (Zeiss) at 80 X. Dissolve BSA powder (fatty acid free) into PBS(-) to obtain 1% (w/v) BSA solution, Dilute collagen type I solution to 0.3 mg/ml with hydrochloric acid (pH 3.0). P-BAM solution: Just before P-BAM solution is applied to the substrate surface, P-BAM is dissolved in DMSO, followed by diluting 100 times in PBS(-). 10-1000 μM P-BAM solution is used for constructing P-BAM surface. Fill 35-mm plastic dish with 1.5 mL of BSA or collagen solution. And then, incubate them at room temperature for overnight. Rinse the coated surface with MilliQ water three times, and then, dry the dish surfaces by incubating at room temperature for more than 1 hour. Place a total volume of avobe 0.5 mL of P-BAM solution onto the dish. After incubation for 1 h at 37°C in a humidified incubator, rinse the dish surface repeatedly with 1 mL of MilliQ water more than six times to remove the unreacted P-BAM.

3.8 Statistical Analysis

Each experiment was repeated three times, and student's t-tests were used to determine statistical significance. $P < 0.05$ was considered to be statically significant. Results were presented as mean ± S.E.M. IC_{50} values were calculated using logarithmic equations.

4.0 Results and Discussions

4.1 The Physical Properties of 3D Microtissues

4.1.1 The Growth of 3D Microtissues as a Function of Time

Figure 10A is a phase contrast image of 3D microtissues composed of Hela cells (a larger area of 3D microtissues composed of Hela cells phase contrast image is inserted). The microtissues are located in the microwell composed of agarose gel, where cells tend to disperse loosely in a 2D surface in the agarose mold which is showed in Figure 10B (size of HeLa cell microtissue as a function of time is inserted). After 24 h, the cells tend to grow into tight 3D structure (Figure 10C).

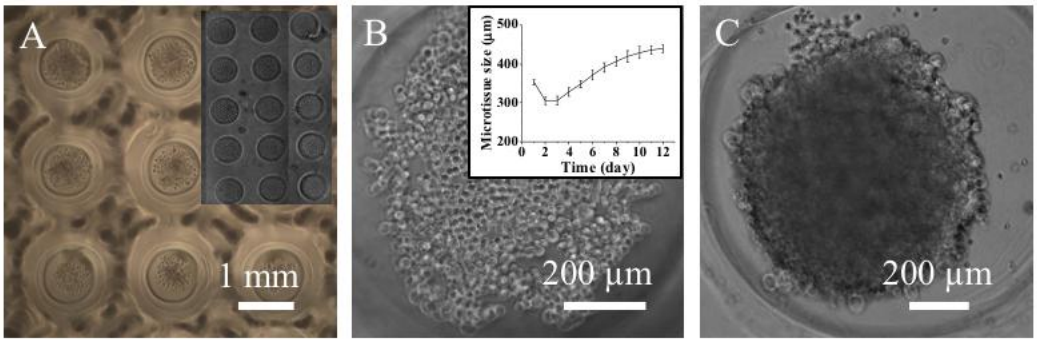

Figure 10: Phase contrast image of 3D microtissues composed of Hela cells (a larger area of 3D microtissues composed of Hela cells phase contrast image is inserted) (A). Phase contrast image of 3D microtissues composed of Hela cell (size of HeLa cell microtissue.

4.1.2 Evaluation of 3D Microtissues

Figure 11D shows a fluorescence image of a microtissue where live cells are green. The absence of red color indicates that cells are alive in microtissue. Figure 11D shows that cells in the microtissues are green indicating cells in microtissues are still alive when cultured in medium for 72 h. The 3D microtissue has stronger green color on its edge and weaker color in the center, probably because the cells are closely packed and it requires longer time for the dye to diffuse into the tissue. Nucleus of the cells in 3D

microtissues are stained with DAPI (Figure 11E), where nucleuses of the cells are very close to each other, indicating the cells in the microtissues are closely packed. The microtissue is stained using ethidium bromide (EB). Figure 12F shows a fluorescence image of a single microtissue taken by using an Olympus BX-51M microscope under ultraviolet excitation, where the spherical shape of the microtissue can be seen clearly.

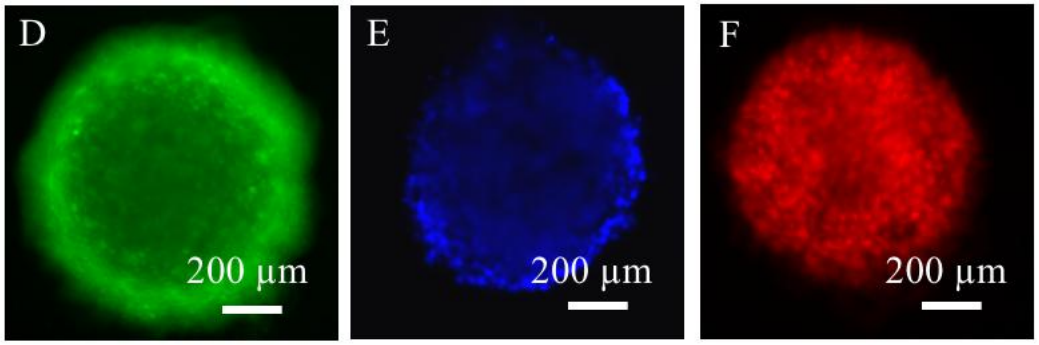

Figure 11: Fluorescence image of a microtissue where live cells are green in color (D). Fluorescent images of nuclei in microtissue (E). Fluorescence image of microtissue stained with EB (F)

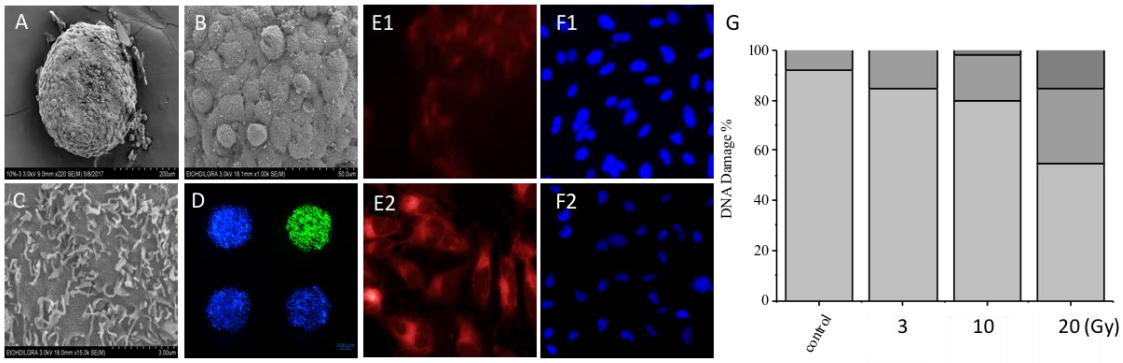

Figure 12: A phase contrast image of the cells seeded into the microwells (A1); A phase contrast image of the cells seeded into the microwells after 2hrs(A2); Bright-field microscopic image of a single-microtissue array(B1); Bright-field microscopic image of a single-microtissue array with different sizes(B2); Fluorescence image of microtissue array stained with DAPI(C1); Fluorescence image of microtissues array stained with DAPI after 10 Gy X-ray irradiation(C2); Different sizes of microtissues array stained with DAPI(D1); Reactive oxygen species (ROS) production after HeLa cell 3D microtissues X-ray irradiation(D2).

The scanning electron microscope (SEM) images of clusters were obtained after formation of the clusters. The scanning electron microscope (SEM) image was obtained by the formation of cluster. With PBS after washing, a cluster is fixed in 2.5% glutaraldehyde solution at 4 ° C for 30 minutes. Osmium tetroxide fixed cluster (OSO4) 2% at 4 ° C 2 h, and deionized water to clean. After the dehydration of the diluted ethanol, the hexamethylsilicate (HMDS) was vaporized and stored in the vacuum chamber before the imaging experiment. Fig. 3A shows the SEM image of the three-dimensional microstructure, revealing that the Hela cells of the microacupuncture are related to and interconnect with the ECM fibers around the surface of the cell membrane. This result indicates that the interaction between cells and cells during the formation of three-dimensional microstructure. The bar size is 100, 15 and 3. Fig.3 shows the two kinds of 3D microstructure arrays, and Hela 3D microstructure is stained by DAPI, while calcein AM staining activity LN229 microsisu green. MitoTracker red CMXRos is a red fluorescent dye that is stained with mitochondria in living cells, and its accumulation relies on membrane potential. After the aldehyde fixation, the dye retained well. Figure 3E2 shows the mitochondrial structure of the untreated cells. In most cells treated with 10 GY x rays in figure 3E1, red spots have fewer structures. X - ray irradiated cells were stained by DAPI and used confocal microscopy to determine the degree of DNA damage. The nuclear structure of the untreated cell is shown in figure 3F1, where the nuclear envelope remains intact and without damage. Figure 3F2 shows the cells treated with 10 GY X-ray radiation, the shape of the nuclear membrane is damaged, and the nuclear content begins to leak. In order to determine the percentage of the damaged nuclear, calculation of at least 60 in each group the nucleus, the result is normalized, as shown in

figure 3 g, in the absence of X-ray irradiation, no serious damaged cells, 7.9% of the cells with moderate damage; In the 3 GY cells, 18.7% and 2.1% of the cells suffered moderate damage, respectively. As the radiation dose increases, more and more cells undergo moderate damage and damage.

4.1.3 The Growth of 3D Microtissues after Radiation

Growth dynamics of the microtissues are characterized by measuring diameter of the area covered by the microtissue. The diameter tends to decrease at the beginning because cells are loosely packed when added into microwell, and tend to form a close structure in the first 2 days. Size of microtissue increase from day 2 due to the division of cells. After day 12, diameter of the microtissues does not increase significantly probably because oxygen and nutrients cannot diffuse into the center of microtissue efficiently. The growth rates of cells in 3D microtissue are studied by measuring the total DNA content of the cells in the microtissue, which is compared to those from 2D cultured monolayer cells. The growth of 3D microtissues is more like in vivo cell growth within human tissues, and this phenomenon can be explained by the shortage of nutrient supply and down-regulation of various growth factors as in solid tumors. Figure 12A1 to 12A4 shows the growth of 3D cell microtissue stained with DAPI without X-ray irradiation from day4 to day12, while 12B1 to 12B4 shows the growth of 3D cell microtissue treated with 10GY X-ray irradiation from day4 to day12. This is consistent with the results reported previously.

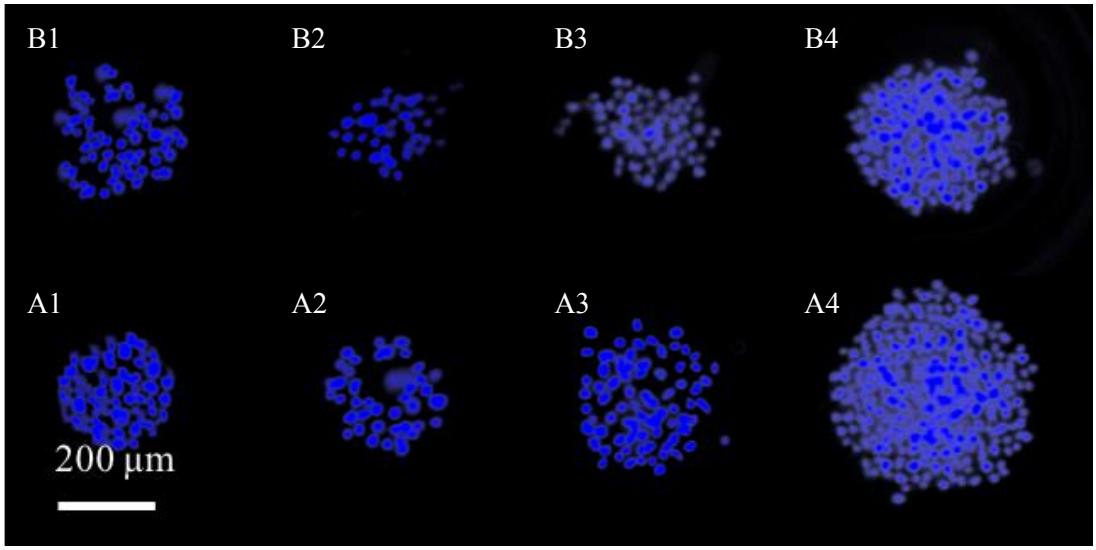

Figure 13: Fluorescent images of nuclei in microtissue with 3GY X-ray irradiation from Day2-Day12 (A1-A4). Fluorescent images of nuclei in microtissue from Day2-Day12 (B1-B4).

4.2 Cellular Detection in Irradiated 3D Microtissues

4.2.1 Nuclear Membrane Assay

Figure A1 shows the morphology of 3D cell microtissue, mitochondria were stained with MitoTracker® Red CMXRos prior to fixation, nuclei were stained with blue-fluorescent DAPI. X-ray irradiated HeLa cells were stained with DAPI and images were taken using confocal microscopy to determine the level of damage to DNA. Figure A2 shows the 3D cell microtissue without X-ray irradiation, where nuclear membrane remain its integrity without damage. Figure A3 shows the shape of nuclear membrane is damaged and nuclear content starts to leak out after exposed to 3GY X-ray irradiation. Figure A4 shows microtissue after exposed to 10GY X-ray irradiation, a larger number of nuclei of cells appeared damaged with a distorted nuclei structure, compared to 3GY X-ray irradiation treatment which is showed in Figure A3.

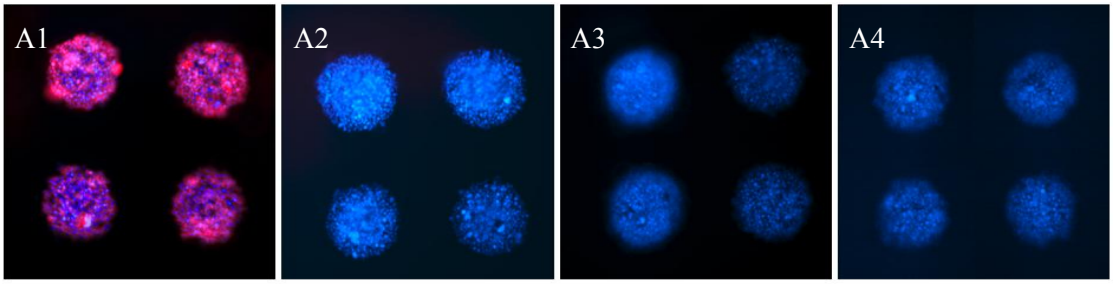

Figure 14: Fluorescent images of nuclei in microtissue (A1-A4).

4.2.2 Micronuclei of 3D Microtissue Assay

Figure 14A1-A3 show the bi-nucleus of cells expressed with or without micronuclei, where Figure 14A1-A3 correspond to cells irradiated with 0GY (Figure 2E1), cells irradiated with 3GY (Figure 14A2), and cells irradiated with 15GY (Figure 14A3) (arrows in Figure 14A1-A3 show micronucleus). The number of micronucleus per 2,000 cells are counted, where cells samples from Figure 14A1, 14A2, and 14A3 have 10, 27, and 59 micronuclei per 2,000 cells, respectively (sample 1 to 3 in Figure 14A4). Sample (2) and (3) have more micronuclei than sample (1), indicating the enhanced chromosome damage by irradiation. Sample (3) have more micronuclei than the other two samples, indicating the enhanced radiation damage by larger dose of X-ray irradiation.

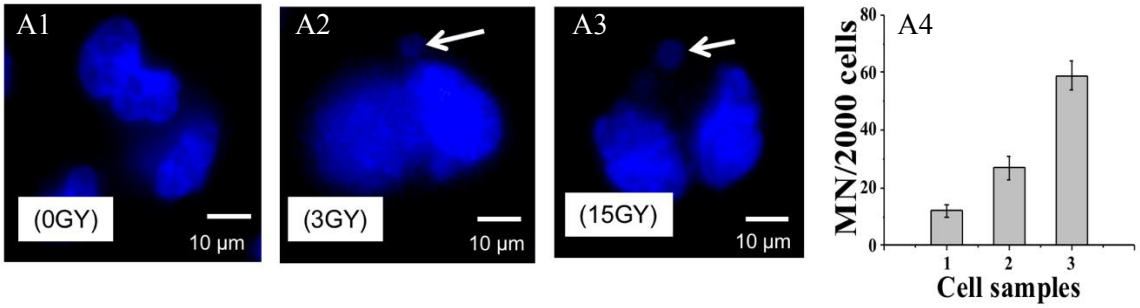

Figure 15: Fluorescence image of cells irradiated with 0GY(A1), with 3GY (A2), with 15GY (A3). MN number of three samples (A4).

4.2.3 Viability Assay

Several factors may contribute to the protective effect in 3D microtissue: (1) reduced surface area of cells exposed to nanoparticles, (2) nanoparticle concentration profile along radial direction of microtissue, and (3) micro-environments in the microtissue. Several factors may have contributed to the protection of the 3 d microstructure: (1) to reduce exposure to the cell surface area of nanoparticles, (2) nanoparticles concentration distribution along the radial direction of the micro organization, and (3) micro organization of microenvironment.

First, the surface area of cells exposed to nanoparticles decreased. For each of the N cells with a radius of r, the total area of the single-layer cells is, if you assume that the single-layer cells are 100% confluence. If these cells are assembled into a sphere of radius R, then the surface area will be. Assuming that the shape and size of the cells do not change, the aggregation and cells of cells in microstructures can be seen as uniform spheres. The ratio of tissue surface area to total cell area exposed to solution is. In 1000 cells, microtissue is 10 times the diameter of cells; Microtissue has a surface area of 20% of a single layer of cells.

Second, when nanoparticles are introduced in a solution containing microtissue, the nanoparticles spread rapidly in solution and spread through the intercellular space to microstructures. Because nanoparticles adhere to the cell surface at a certain rate, the number of nanoparticles along the radial direction gradually decreases.

Finally, the cells in the outer layer of the microstructure have more nanoparticles than the center cells, so the cells in the middle are less damaged. In 2D culture, each cell is exposed to the same amount of nanoparticles evenly, so the damage to each cell is the same.

The diffusion process of free radical infiltration to microstructure was studied to help explain its protective effect. In addition, microenvironment is another important factor influencing toxicity results. The phenotype and function of individual cells are highly dependent on the complex interactions of the extracellular matrix (ECM) proteins and adjacent cells in three-dimensional tissues. ECM protein may play an important role in the toxicity tolerance of 3D microtissue culture, as they form a natural barrier to limit the diffusion of nanoparticles. It is reported that the surface of HepG2 tissue is covered with a well-developed ECM layer, which is common in all tissues and can reduce the penetration of methotrexate. In addition, cell function is well maintained in microtissue culture. Compared with 2D culture, cells in 3D microstructure may enhance repair ability or damage tolerance. Similar phenomena were observed in hepatocellular microstructures.The diffusion process of free radicals penetrating into the microtissues is studied to help explain the protective effect. In addition, microtissue microenvironment is another important factor affecting the toxicity results. The phenotype and function of individual cells are highly dependent on sophisticated interactions with 3D organized

extracellular matrix (ECM) proteins and neighboring cells. ECM proteins may play important roles in the toxicity tolerance in 3D microtissue culture because they form a natural barrier that limits the diffusion of the nanoparticles. It has been reported that the surface of HepG2 microtissue is covered by a well-developed ECM layer, which is common for all tissues and can reduce the penetration of methotrexate. Moreover, the cellular functions are well maintained in microtissue cultures, and it is possible that cells in 3D microtissue will have enhanced repair ability or damage tolerance compared to those in 2D culture. Similar phenomena have been observed in hepatocyte microtissue.

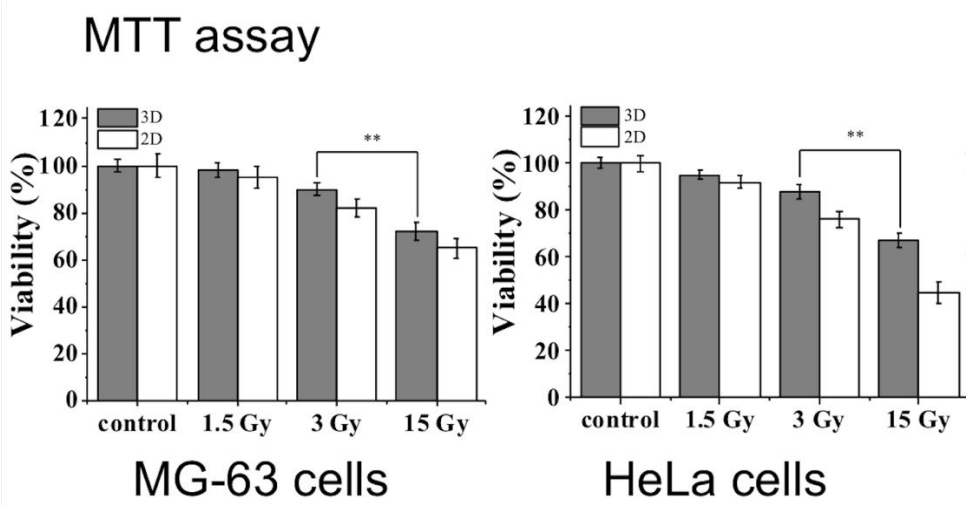

Figure 16: MTT assay viability assay result.

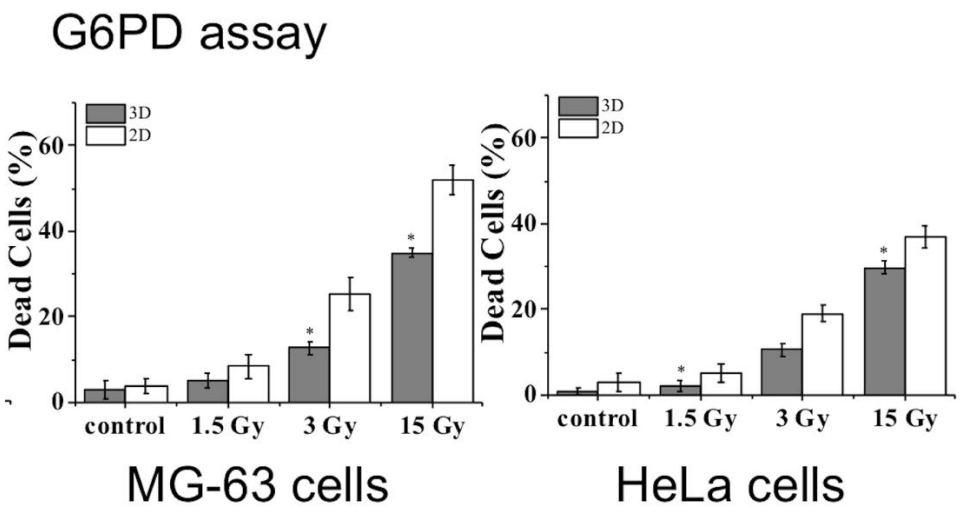

Figure 17: G6PD viability assay result.

4.2.4 Radiation Biodosimetry with 3D Microtissue

MTT assay was performed on MG-63 and HeLa cells to assess their viability following irradiations. Figure 17A shows the continuous irradiations kill more cells in the HeLa microtissue than the cumulative irradiations, especially when the irradiation time is longer than 3 h. The difference in cumulative and continuous exposures is mainly caused by self-repairing of small amounts of DNA damage. Cumulative exposure provides time for the damaged DNA to self-repair between exposures while in the case of continuous exposure the damage accumulates faster than it can be repaired in 3D cell microtissue. Figure 17B shows the continuous irradiations kill more cells in the HeLa microtissue than the cumulative irradiations, especially when the irradiation time is longer than around 3 hours.

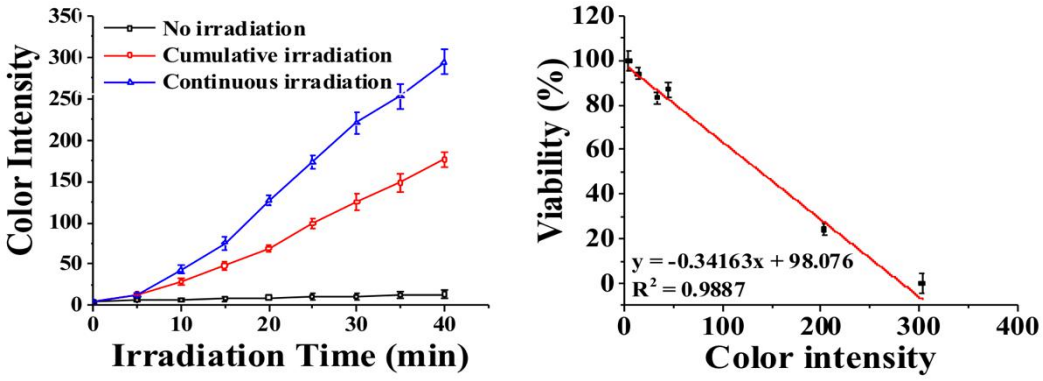

Figure 18: Color intensity of trypan blue stained HeLa microtissues for continuous and cumulative X-ray exposures (A). HeLa cell viability against the color intensity of trypan blue stain (B).

4.2.5 Diffusion Ability of Different Modified Nanoparticles

Examination of different modified nanoparticles diffusion effect on the 3D microtissues. For diffusion assay, the microtissues will be treated with 200 μg/ mL Gold nanoparticles (Au, Au-PEG, Au-PEG-CPP). The solution will be pipetted out at 10 min intervals for nanoparticle concentration measurement (XRF or fluorescence). For 2D cell culture, the same cell suspensions will be prepared and 200 μL of HeLa or MG-63 cell suspension will be seeded with final concentrations of 1 × 105 cells/mL in each well and cultured in an incubator with 5% CO2 at 37°C. After the monolayer of cells become 80% confluent, the cells will be incubated with nanoparticles (Au, Au-PEG, Au-PEG-CPP) in fresh medium at final concentrations of 2, 20, and 200 μg/mL. After 24 h, the medium in each well will be removed and all wells were washed with PBS prior to any toxicity assays. To detect whether X-ray radiation can affect cellular function.

4.2.6 X-ray Radiation on Nanomedicine Diffusion on 3D Microtissues

To detect the effect of X-ray radiation on nanomedicine diffusion on 3D microtissues, the 3D microtissues will be exposed to different dose of X-ray radiation. From 0 GY, 1.5 GY, 3 GY to 15 GY. Then G6PD (glucose-6-phosphate dehy-

drogenase), calcein AM/EthD-1 (calcein AM and ethidium homodimer), and MTT [3-(4,5-dimethylthiazol-2-yl)-2,5-diphenyltetrazolium bromide] assays will be performed following suppliers' instructions. As for MTT assay, the medium in each well will be removed and replaced with 100 μL of fresh medium. Ten microliters of 12 mM MTT stock solution will be then added into each well and into a negative control (100 μL of medium without nanoparticles). After incubation at 37°C for 4 h, 100 μL of SDS−HCl solution will be added in each well and mixed thoroughly via pipet. The cells will be lysed by adding 1 μL cells lysis buffer into the well. All samples will be assayed in six duplicates. The microplate is incubated at 37 °C for 30 min prior to measurement of fluorescence intensity at 580 nm with 530 nm excitation. For calcein AM/ EthD-1 assay, 100 μL of D-PBS is added in each well to wash cells to dilute serum-containing esterase.

4.2.7 O_2 Diffusion affect Radiation Damage to 3D Microtissues

Two human cancer cell lines, HeLa (cervical cancer) and LNCaP (prostate cancer) are obtained from the American Type Culture Collection (ATCC Manassas, VA) and cultured in standard conditions (5% CO_2 in air at 37 °C) in RPMI-1640 medium, Two human cancer cell line hela (cervical cancer) and LNCaP (prostate) from American type culture collection (ATCC manassas, Virginia) and to develop under standard conditions (5% of carbon dioxide in the air at 37 ° C) in rpmi - 1640, added 10% fetal bovine serum (v/v) and 1% (v/v) of penicillin and streptomycin. In my culture cell culture medium (Lonza Walkers - ville MD), added 1% (v/v) of penicillin and streptomycin, 1% (v/v), 10% (v/v) fetal bovine serum under standard conditions (5% of carbon dioxide in the air at 37 ° C). Cells are cultured every three to four days, and all cells are used between channels. D - the cells will be twice PBS and resuspended fresh new media in 6 - well 1 x

105 / set contains each of the different drugs (etoposide, hydrochloric acid, hydrochloric acid doxorubicin stand for kang) in different concentrations (0.05, 0.1, 10, 50 microns) and 2.0 h hatch standard culture conditions. After the drug is washed, the cells will be loaded onto a patterned substrate to form a cell array. DNA damage will be determined by an improved basic halo analysis, as described below. Briefly, after coagulation of agarose sugar, 0.3 M sodium hydroxide was incubated for 30 minutes at room temperature and 10 min. G/ml EB for 10 minutes. The slide is incubated for 5 minutes. The fluorescent image was taken in an Olympus microscope (BX51M) and an Olympus ColorView CCD camera. The image analysis software (image J) will be used to obtain the halo and the size of the nucleus from the captured image. Each cell's rNDF value will be derived from halo and nucleus. Untreated cells will be used as negative controls. Data statistical analysis was performed using SPSS 19.0 (SPSS Inc., Chicago). The drug inventory solution can be prepared by dissolving the appropriate amount with the dimethylsulfoxide solution and obtaining the required concentration. All chemicals can be used without further purification. Mixed gas (N2:CO2:O2 = 93%:5%:2%) is from the U.S. air liquide (Orlando, FL).

4.2.8 O_2 Diffusion affect Radiation Damage to 3D Microtissues

If Quantifying single cell DNA damage/repair time using different cell line, the cells are then loaded onto the patterned substrate to form single cell arrays. If individual cell DNA damage/repair time is quantified with different cell lines, then the cells will be loaded onto a pattern-based substrate to form a single cell array. The electrostatic attraction between a positively charged pattern and a negatively charged cell membrane attracts the cells through electrostatic attraction. The cells were then implanted in agarose

gel and tested for DNA damage and repair by HaloChip, as shown in the figure below. After agarose solidifies, the slide is incubated with 0.3 M sodium hydroxide for 30 minutes at room temperature, and 10 minutes for 10 minutes of g ml. The slide will incubate for 5 minutes to remove free dye. The fluorescent images will be taken using the Olympus microscope (BX51M) and the Olympus ColorView CCD camera. Using the image analysis software (Scion image) to obtain the halo and core size from the collected images, rNDF = R2/ R2 is used to calculate the rNDF values of each cell, where R and R are respectively the diameter and core of the halo. The drug concentration will be selected according to the clinical dosage. Each experimental point averages at least 50 cells, and the data represents the mean. Untreated cells will be used as negative controls. In the case of repair, drug treatment of cells with PBS and incubation medium at 37 ° C before determination of different time intervals. Damaged cells that do not have time to repair will be used for control. Repair data will return to install and use the first-order index equation: one is the DNA damage of time 0 D (t) the DNA damage of time t, tau is reversible, depending on the time constant repair rate and c is the residual of repair damage from extrapolation. T is 50 queries to reduce DNA damage by 50% and use t50 =(2).

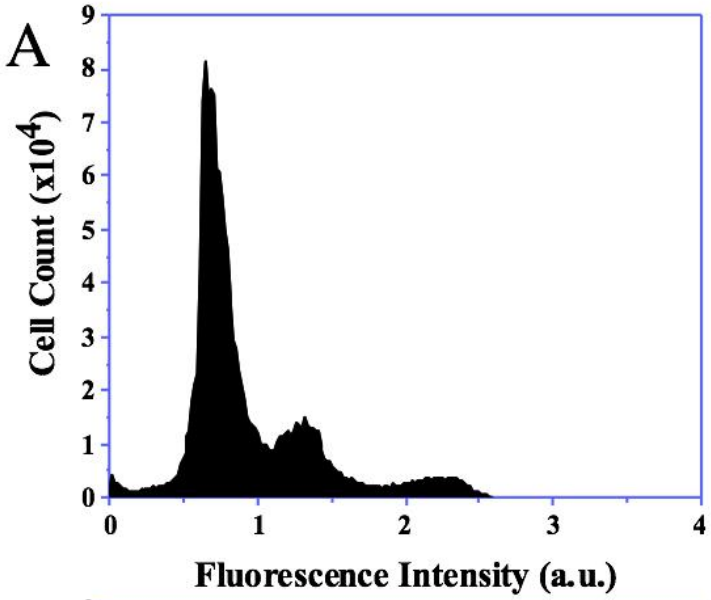
A
Cell Count (x10^4)
Fluorescence Intensity (a.u.)

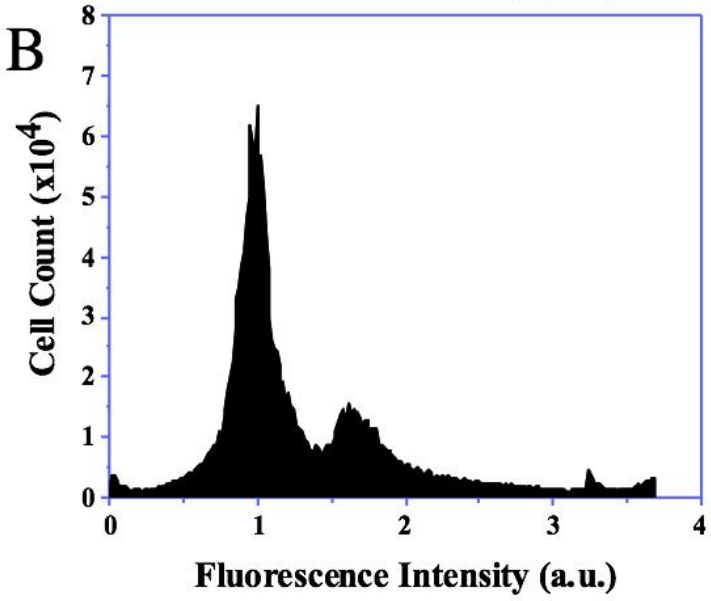
B
Cell Count (x10^4)
Fluorescence Intensity (a.u.)

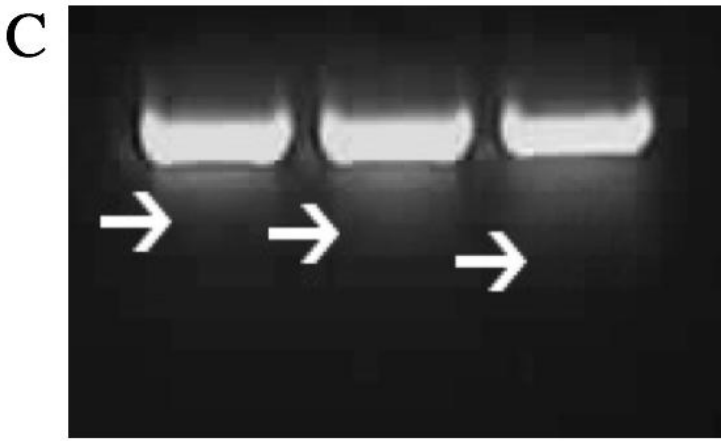
C

Figure 19: X-ray induced DNA damage of cells without X-ray(A) and with 15 Gy X-ray irradiation(B); gel electrophoresis results of three samples (bands from left to right are from sample 1 to sample 3);

4.3 Genomic Detection in Irradiated 3D Microtissues

4.3.1 Halo Assay

The use of radiation damage of cells has been assessed at single cell level with HaloChip assay as follows: 3D micro tissues (a diameter around 250 μm) with X-ray radiation for 3mins and 10 mins. The cells in the microtissues are re-dispersed into isolated cells by trypsinization. To form single cell array, positively charged polyelectrolyte multilayer array is formed on glass substrate for attaching cells. The polyelectrolyte multilayer array is prepared by microcontact printing and layer-by-layer assembly. Briefly, a layer of PDAC is absorbed onto PDMS stamp bearing micropillar array via hydrophobic interaction. Another two layers of polyelectrolyte, PSS and PAH-RITC, are then attached onto the PDMS stamp via electrostatic interaction. The PDMS stamp is washed after depositing each polyelectrolyte layer so as to remove excess polyelectrolyte molecules. The stamp is then printed onto a glass slide to form ordered polyelectrolyte array. Cells are attached to the polyelectrolyte array through electrostatic interaction and then embedded in agarose gel. After gel solidification, the sample is immersed in an aqueous solution of NaOH for lysis. Damaged DNA fragments self-diffuse into gel matrix, and are stained with SYBR green fluorescence dye, forming a diffusive ring around each nucleus (Figure 18A). DNA damage is quantified with relative nuclear diffusion factor (rNDF), which is derived from areas of halo and nucleus as follows: $rNDF= (R^2-r^2)/r^2$ where R and r are the radii of halo and nucleus, respectively

(Figure 18A). Figure 18A-C are halo arrays of three types of samples: cells irradiated for 0 GY, cells irradiated for 3 GY, and cells irradiated for 15 GY (Figure 18C), where their rNDFs values are samples #1 to #3 in Figure 18D: sample (1) has smaller rNDFs than the other two; sample (3) has larger rNDFs than sample (2), indicating the enhanced DNA damage by larger dose of X-ray irradiation. Since rNDF is related to DNA double strand breaks, these results confirm the radiation damage to 3D microtissues.

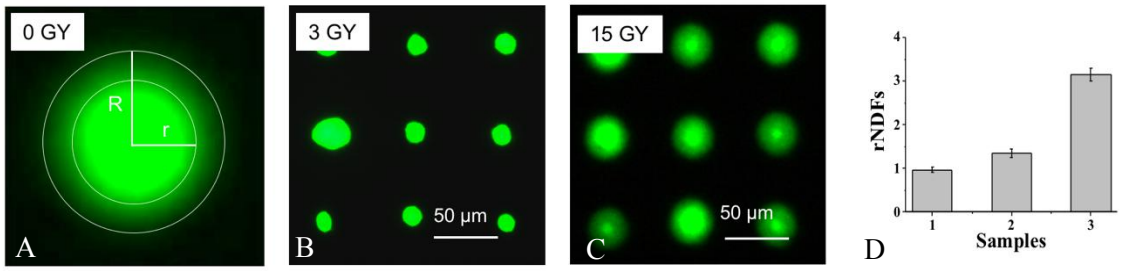

Figure 20: The fluorescence image of damaged DNA fragments (A). Halo arrays of cells irradiated with 3.0 GY (B). Halo arrays of cells irradiated with 15.0 GY (C). The rNDFs values of three samples (D).

4.3.2 The Expression of DNA Repair Protein (γ-H2XA)

The effect of X-ray radiation damage to DNA has been assessed at protein level by measuring the expression of a DNA repair protein, γ-H2AX, which is recruited to the DNA double strand breaks sites for repair. Briefly, the 3D microtissues are subjected to X-ray irradiation except for the control. Cells in the microtissues are re-dispersed into isolated cells by treating microtissues with trypsin and pipetting the medium up and down. The cells are washed with PBS. Primary and secondary antibodies are added sequentially into cells. The secondary antibody is conjugated with fluorescein, which allows fluorescence imaging and quantification of γ-H2AX expression by measuring

fluorescence intensity. Cells irradiated with 1.5GY show weak green fluorescence (blue color is due to DAPI staining of DNA), indicating a small amount of γ-H2AX is expressed (Figure 19C). Cells irradiated with 10GY show stronger γ-H2AX expression than irradiation 3GY, indicating increased expression of γ-H2AX is expressed (Figure 19C). The fluorescence signal from DAPI stained DNA is artificially reduced to highlight green color. The green fluorescence intensities of cells have been quantified with 96 well plate reader. Figure 19A shows the fluorescence intensities of (1) cells irradiated 0GY, (2) cells irradiated with 3GY, and (3) cells irradiated with 15GY. Sample (1) has lower fluorescence intensity than the other two samples; sample (3) has higher fluorescence intensity than sample (2). Because γ-H2AX is related to DNA double strand breaks, these results confirm radiation can enhance radiation induced double strand break of DNA.

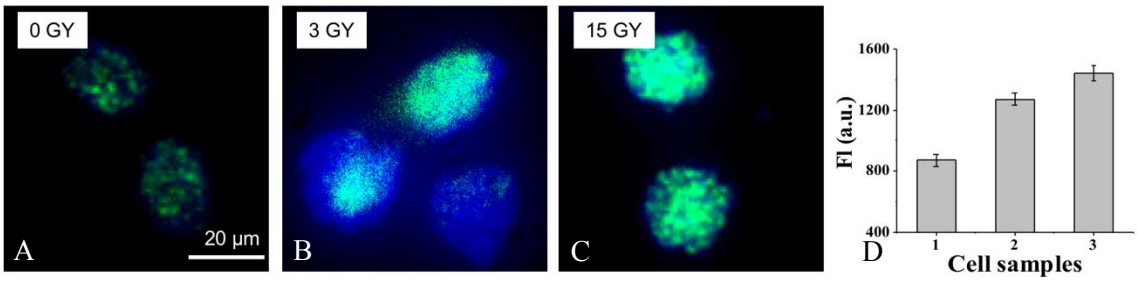

Figure 21: Fluorescence image of cells without radiation (A), with 3GY (B), with 15GY (C). The integrated intensity of florescence of three samples (D).

4.3.3 The Expression of α-tubulin and vinculin

Protein expression of the cells in the NFC film matrices were conducted by using the Red and Green Fluorescent Protein (α-tubulin and vinculin). Blue color indicates nuclei stained by DAPI in Figure A1. Figure A2 and A3 shows the extensive microtubule network of untreated cells. This phenomenon correlates with a healthy cell where cargo-carrying motor proteins used the microtubule network to move essential proteins intracellularly. In one experiments, cells were seeded on the NFC matrices.

There are more cells in Figure B1. As shown in the fluorescent images (Figure B2 and B3) and the fluorescent imaging analysis (Figure C), the expression of corresponding fluorescent proteins α-tubulin and vinculin in Hela cells were promoted in the existence of the NFC matrices, indicated by the intense distribution of the two proteins. The enhanced cell proliferation rate in the presence of NFC matrix can also lead to the increase of protein expression. It suggests that the NFC-based matrices can promote not only the cancer cell growth and proliferation, but also the transfection of exogenous DNA into the cells. Figure A4 and B4 show merged images of A1-A3 and B1-B3, respectively. The florescence integrated intensity of sample A3 and sample B3 is showed in figure C, where yellow and orange bars represent α-tubulin and vinculin, respectively. Figure D shows the proliferation of cells seeded on the NFC matrix and without NFC matrix.

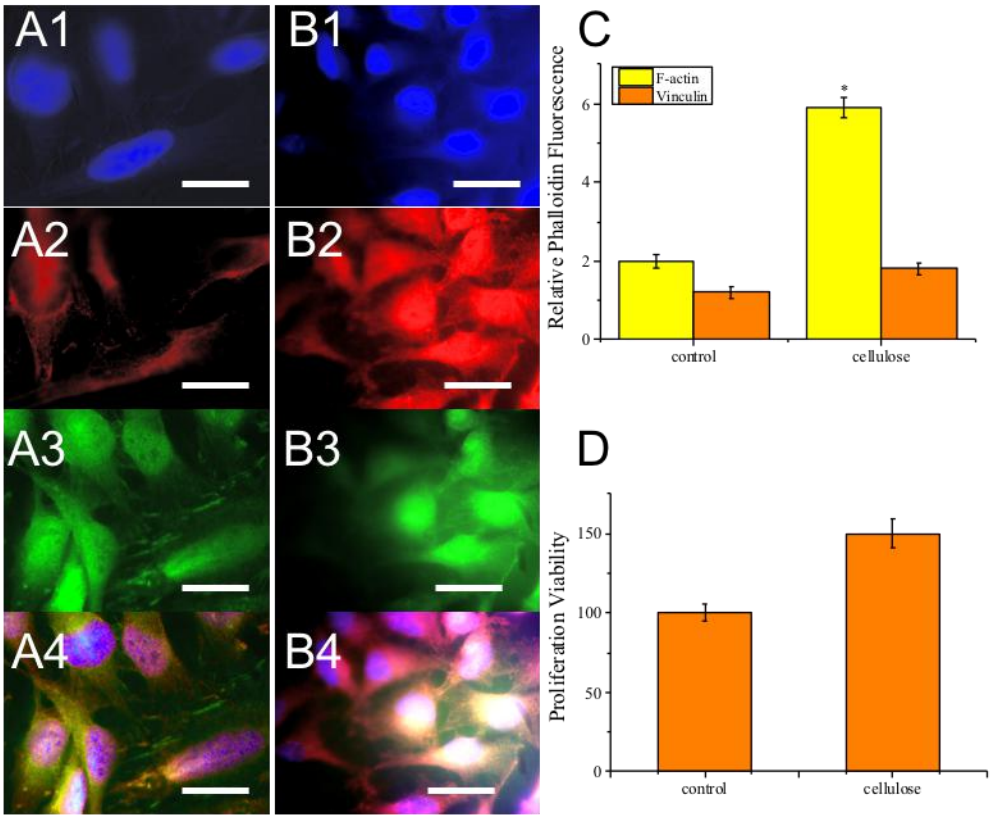

Figure 22: Fluorescence image of cells without radiation (A1-A4), with 3GY (B1-B4), with protein expression (C). The integrated intensity of florescence of three samples (D).

Figure A1 fluorescence image of a single microtissue taken by using an Olympus BX-51M microscope under ultraviolet excitation, where the spherical shape of the microtissue can be seen clearly. FIG. A1 is a fluorescence image of a single microstructure captured using the Olympus bx-51m microscope under ultraviolet light, and the spherical shape of microstructure can be clearly seen. In order to determine the viability of cultured microtissue cells, a fluorescence staining was performed by Calcein AM, and Calcein AM stained live cell green, leaving dead cells unchanged. Software such as Python and MATLAB can effectively deal with images of single cell ordered arrays. We first used Python to process the quantified fluorescence intensity of each array image and individual cell. This method is based on splitting the image into the same area,

and each region contains only one cell. Then the information in each region is analyzed. Calculate the average strength of each pixel in the region and calculate the cell strength in the region. FIG. 2 shows a fluorescence image of living cells as green microstructures. No red indicates that cells live in microtissue. Due to micro nutrients and oxygen content of tissue within the cell is limited, a growth in the supportive tissue of the micro speed slower than the speed of the single micro organization, outside the incubator of fresh medium survival time of more than 96 hr, makes the micro organization of field expandable radiation detection has great attractive. A viable way to live longer is to grow cells in a normal single-layer mode, forming microstructures within hours of radiation detection. Figure A1-B2 and b1-b2 show histogram of the fluorescence intensity distribution of cells before and after radiation, and DAPI and calcein are respectively stained. Figure A3 and B3 show the combined images of a1-a2 and b1-b2 respectively. In figure C, the black column represents samples treated with a 20Gy X-ray, and the red pillars represent unprocessed samples. It shows the statistical distribution of fluorescence intensity of living cells. The total fluorescence intensity of the untreated samples was 5.3 times of the 20Gy x - ray exposure sample. FIG. E and F show cell diameter distribution and 20 Gy x ray irradiation without X-ray irradiation, and more cell debris after X-ray exposure.

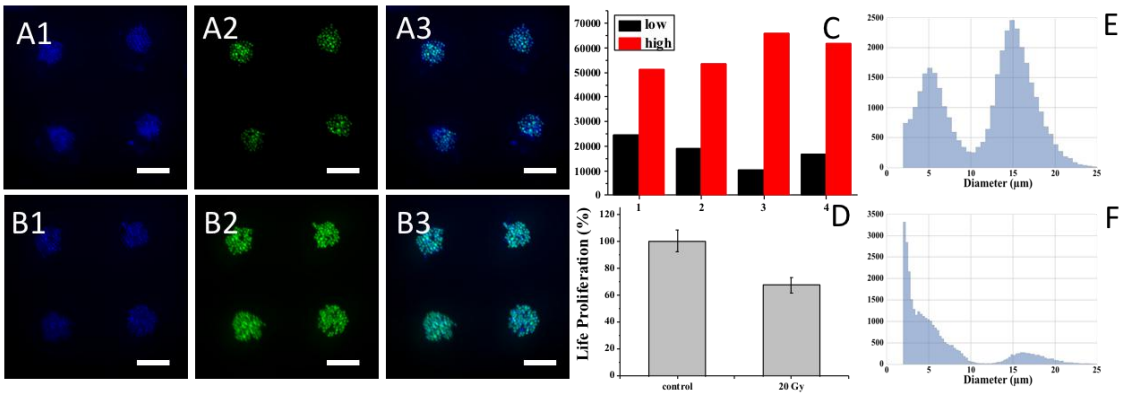

Figure 23: Fluorescent images of microtissues stained with DAPI(A1); Live cells are stained in green in microtissues(A2); Merged fluorescent image(A3); Fluorescent images of microtissues stained with DAPI with 20Gy X-ray irradiation(B1); Live cells are stained in green in microtissues with 20Gy X-ray irradiation(B2); Merged fluorescent image(B3); The statistical distribution of fluorescence intensity of live cells(C), 20Gy X-ray irradiation (black columns) and un-treated samples (red columns); Life proliferation of 3D microtissues(D); The distribution of cell diameter without X-ray irradiation(E) and with 20Gy X-ray irradiation(F).

4.4.1 Migration of 3D Microtissues in Matrigel

The result that as the X-ray dose increases, the speed of migration decreases, The speed of migration decreases with higher concentration of AuNPs.

B

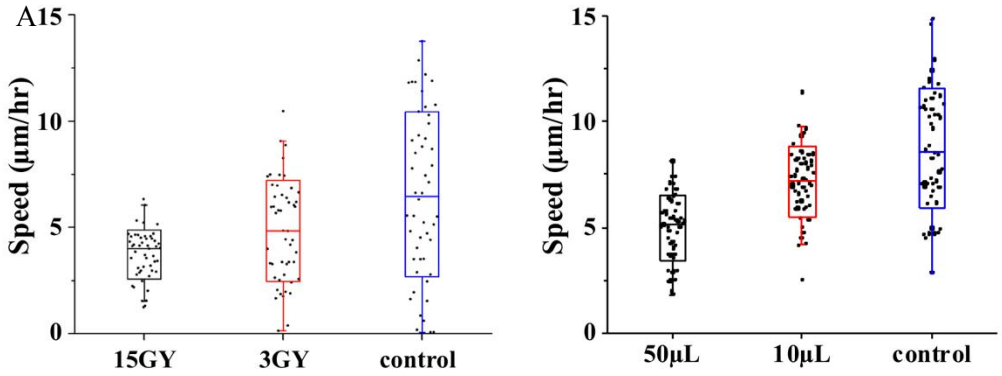

Figure 24: The migration of 3D microtissues under different X-ray dose (A). The migration of 3D microtissues with different concentration of PEG-CPP-AU nanoparticles (B).

4.4.2 Migration of 3D Microtissues in Matrigel

To mimic the 3D ECM scaffolds for 3D cell culture study and for tissue engineering application, the biocompatibility and efficacy of the NFC-based matrices should be assessed. Therefore, the first goal was to test the functionality of the generated matrices in supporting cell survival. The second goal was to assess the capability of the generated matrices in promoting cell proliferation, which is critical in tissue engineering and tumor study. The epithelial-derived Hela cells which was widely used for tumor studies, was applied to assess the biocompatibility of the NFC-based matrices. In order to determine viability of cells in the microtissue, live/dead assay with fluorescence staining is carried out with Calcein AM, where Calcein AM stains live cells green leaving dead cells unaltered. Figure A1-A4 shows fluorescence images of a microtissue where live cells are green. The 3D microtissue shows stronger green color on its edge and weaker color in the center, probably because cells are closely packed and it requires longer time for dye to diffuse into the tissue. Growth dynamics of the microtissues seeded on NFC matrix are characterized by measuring diameter of the area covered by microtissue which are showed in figure B1-B4, while figure C1-C4 shows the growth of 3D microtissue without

NFC matrix. The nuclei of cells in 3D microtissues are stained with DAPI, where the cell nuclei are close to each other, indicating close packing of cells in the microtissues. Integrated green fluorescence of A1-A4 is showed in figure D. Figure E shows the integrated fluorescent intensities of two samples (B1-B4 and C1-C4), where the color intensity of microtissues seeded on the NFC matrices is higher than those of non-seeded on NFC matrices. Figure F shows the size of microtissue increases as a function of time, where 10-12 days of culture can produce uniform HeLa microtissues with an average size of 400 μm, at the initial seeding concentration of 105 cells/mL. The microtissue non-seeded on NFC matrix follows the similar growth pattern, but the grow rate is lower compared with microtissues seeded on the NFC matrices. These results suggest that the NFC-based materials are promising candidates as matrices for 3D cell culture study and other tissue engineering applications. Moreover, the charge density of cellulose fibers and the material processing approaches were found to moderately affect the cell proliferation.

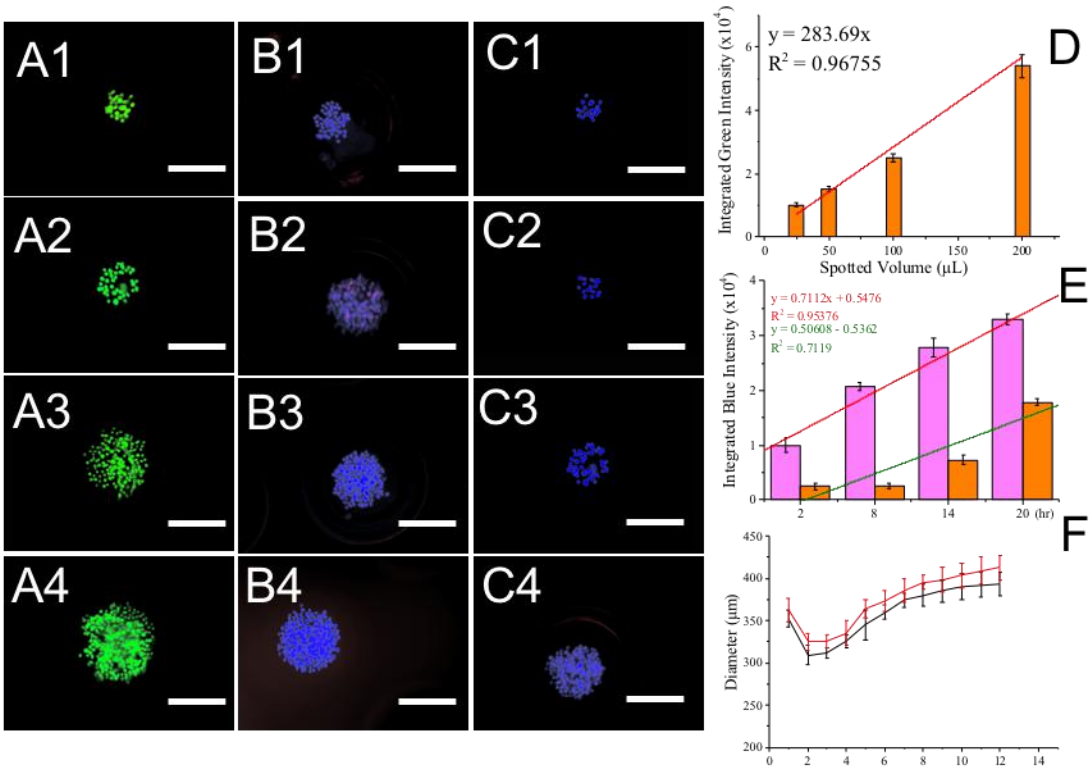

Figure 25: The migration of 3D microtissues under different X-ray dose (A1-A4). The migration of 3D microtissues with different concentration of PEG-CPP-AU nanoparticles (B).

Forces generated in the actin cortex help move a cell forward. actin polymerization at the leading edge of the cell pushes the plasma membrane forward (protrusion) and forms new regions of actin cortex, shown here in red. The force of the actin cortex helps the cells move forward. The actin polymerization in the leading edge of the cell pushes the plasma membrane forward and forms a new area of the actin cortex, shown here in red. The strength of the actin cortex helps the cells move forward. The actin polymerization in the leading edge of the cell pushes the cell membrane forward, forming a new actin cortical area, which is represented here in red. A new anchor is formed between the bottom of the cell and the cell surface (attachment). When the myosin movement protein moves along the actin membrane, the tail of the cell contracts

and then pulls the cell's body forward. The new anchor is anchored in front, and the old anchor is released behind because the cells are moving forward. The same cycle repeats again and again, allowing the cells to move forward in a gradual manner. Unit migration is a carefully choreographed multistep process. (a) through the aggregation of actin filaments, the first migrated cell becomes polarized and extends to a significant structure; (b) due to the combination of the integrin and extracellular matrix, relatively weak newborn adhesion was formed under the lamina; (c) the tension produced by the stress fibers causes the nucleus and cell body to move forward; (d) the cells contract through instability and the focal adhesion that is released in the region.

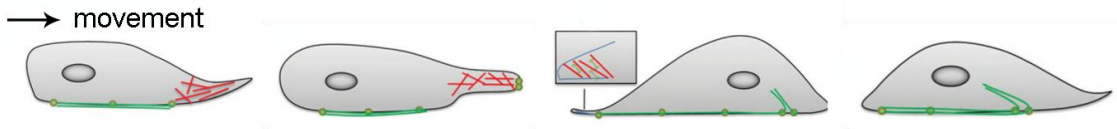

Figure 26: The migration of 3D microtissues in gel.

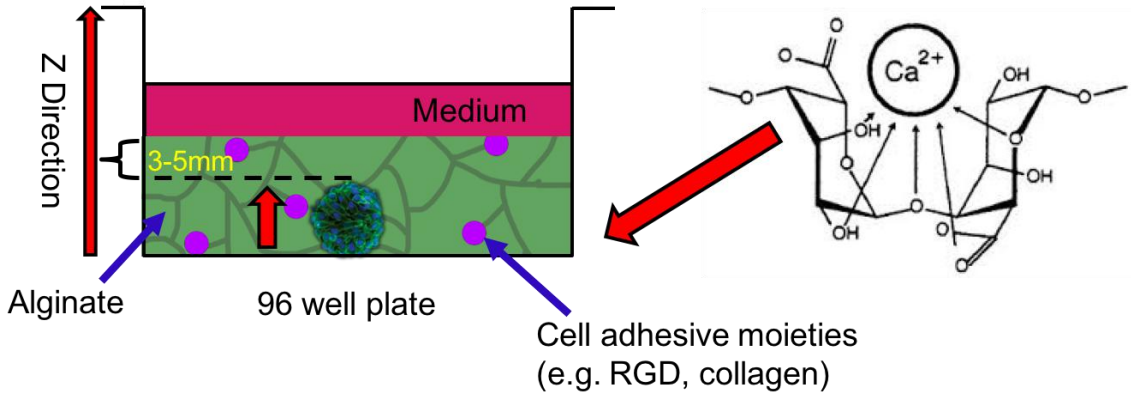

Figure 27: The migration of 3D microtissues in gel.

For migration, we want to detect migration on a three-dimensional microenvironment and a two-dimensional surface. Although biochemical factors such as adhesion receptor

and the ligand concentration and combination, through the signal transduction, cell adhesion complexes and remove, the structure of the cytoskeleton in 2 d environments have a detailed research, and the three dimensional stromal cells migration key biochemical and biophysical parameters without quantitative research. We prove that, in addition to adhesion and tactile force, the stiffness of the matrix is the key factor affecting the motion of three-dimensional cells. Cell migration experiments show that the migration rate of cells is a balance between scaling and adhesion in a specific matrix density. However, when the biochemical parameters such as the matrix ligand and cell integrin receptor remain unchanged, the largest cell movement is transferred to the weaker matrix. This behavior is inconsistent with the current two-dimensional model, but in the three-dimensional matrix, the latest computational model of the force based cell movement predicts this behavior. As expected, the three-dimensional motion, which is much smaller than the cell size, relies on proteolytic activity through the extracellular environment, because the wide spectrum of MMP inhibitors limit the migration of cells. Alginate can be treated by Ca and can control the distance and time of microstructure movement. RGD - modified alginate gel is the most commonly used in vitro cell culture matrix. In alginate gels, RGD peptides can control the phenotype of the interacting muscle cells. For example, compared with non-modified alginate gel, alginate gels adhered to and proliferated with the chemical coupling agents of RGD peptides. In addition, the number of cells adhered to the gel and the growth rate were closely related to the large amount of RGD density in the gel. The distance arm length between RGD peptide and alginic acid chain is an important parameter to regulate cell response. The adhesion and growth of the primary human fibroblasts with alginate gel and GnRGDSP

sequences were not related to the total concentration of polypeptides in the gel. The dependence of three-dimensional microstructure migration on matrix density was detected. The three-dimensional microstructure is added to the matrix of different concentrations. Cell movement in hydrogels. These cells show rapid movement in the hard hydrogel, because the increase in the strength of the gel increases the adhesion of the compound, such as integrin. In addition, integrin receptors and fibronectin seem to play an important role in migration and invasion. In order to detect the dependence of three-dimensional microstructure migration on matrix density.

4.4.3 Migration of 3D Microtissues in Matrigel

In human body, the stiffness of three-dimensional matrix is an important factor for cell growth and differentiation. In human body, the stiffness of three-dimensional matrix is an important factor for cell growth and differentiation. More importantly, microenvironment can regulate cell function and tissue integrity, including migration and change of cell and cell matrix adhesion. The resilience and hardness of tissue are reported to be related to cancer biology. For example, the progression of cancer in soft tissue is related to the hardness of local accumulation, usually caused by cross-linking collagen matrix caused by the physical interaction of the tumor. Collagen gel with different matrix density was prepared. In order to study the different substrates simulated in human body system, the collagen concentration of 2, 4, 6 mg/mL was used in this study. Collagen gel energy storage modulus at 30 ° C prepared from collagen solution/Pa 200-400800-1800 and 400800-200-2 mg/ml concentration, respectively. The morphological changes of clusters in collagen gel were observed by using a living cell confocal microscope. The cell migration was measured at 20 points and defined by the distance from the cluster

center 48 hours later. The concentration of collagen gel was small, but the cell migration was affected. The cell migration amount of collagen gel was 4 mg/ml(837.6 + 89 mm), compared with the larger cell collagen gel concentration of 2 mg/ml(745.0 + 96) or 6 mg/ml(800 + 87 mm). Many research groups have studied the reactions of cell movements in hydrogels. These cells show rapid movement in the hard hydrogel, because the increase in the strength of the gel increases the adhesion of the compound, such as integrin. In addition, integrin receptors and fibronectin seem to play an important role in migration and invasion. Therefore, the study found that tumor cells were affected by the concentration of collagen gel from microtissue migration.

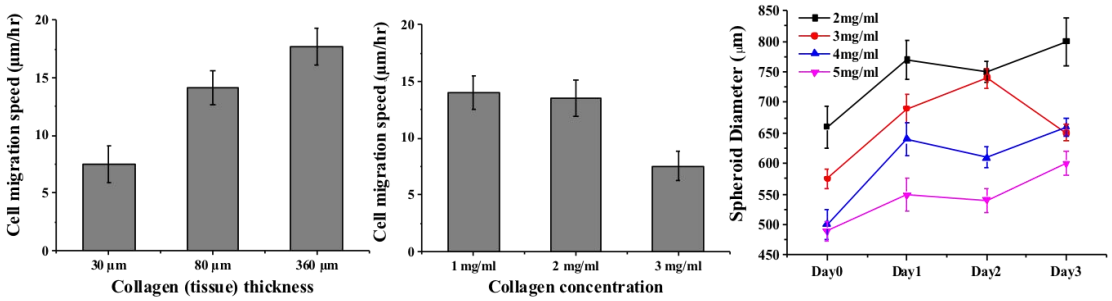

Figure 28: 3D microtissues migration in different thickness of collagen (A). 3D microtissues migration in different concentration of collagen (B). The spheoid diameter depent on the time from day1 to day3 in different concentration of collagen.

4.4.4 Migration of 3D Microtissues in Matrigel

The collective cell behaviors are defined as an orchestrated movement among interconnected cell groups. It is exploited by cancer cells as an efficient invasion strategy that can be modeled in the laboratory. The ECM remodeling surrounding the cells, resulting in a topological rearrangement of ECM fibers that in turn shape the tissue

microenvironment or promote invasive phenotypes. The formation of ECM fiber might be improved by their biophysical interaction of the cell-ECM-cell contact and cell-matrix adhesion. Transwell assay in the migration assay is often used to examine the migratory response of cells. Cells are placed on the upper layer of a cell permeable membrane and a solution containing the test agent is placed below the permeable membrane.28-29 Following an incubation period of 4-24 hrs, cells that have migrated through the membrane are stained and counted. The membrane is often coated with extracellular matrix component (such as collagen) which facilitates both adherence and migration. Figure A shows a cell monolayer formed on matrigel with cell density of about 1.1×105 cm2. Figure B shows image of cells that have been treated with PEG-CPP modified nanoparticles (20 μM) and exposed to 0.75 GY radiation. The number of cells passing through the matrigel is largely reduced with a surface density of 8×104 cm2. Figure 4C shows nanoparticle treated cells after exposing to 3 GY radiation, where the number of cells passing through the matrigel is further reduced to 3×10^4 cm2. Figure D summarizes the results, where cells treated with nanoparticles have the highest number, while cells treated with both X-ray radiation and nanoparticles have the lowest number. I50 result is showed in Figure E. Figure F shows the MFI of each sample: cells with gold nanoparticles exposed to 3 Gy, cells with gold nanoparticles exposed to 15 Gy, cells without X-ray irradiation. Cell death (apoptosis) under different treatments has also been determined using flow cytometry. A number of cells with gold nanoparticles are exposed to X-ray irradiation for different times, and cultured in medium for 48 h. Dead cells in medium are collected, enriched by centrifugation, stained with PI, and counted by flow cytometry. As the irradiation time increases from 0 to 15 Gy, more cells are killed

(Figure G). microtissue diameter treated with collagen concentration of 2, 3, 4, 5mg/ml (from up to down), where microtissues growth decreases as the collagen concentration increases. The diameter of microtissues generated by different numbers of cells (from 0K to 40K) is showed in Figure B. Cell number of microtissues after exposed to 0, 3, 15 Gy X-ray irradiation is showed in Figure C. DNA damages in the four samples are assessed by electrophoresis, where cells are treated with 0.3 M NaOH for 10 min, and DNAs are stained with ethidium bromide (EB). DNA damages are quantified by distances that DNA fragments move in gel electrophoresis. Figure D shows that DNAs after microtissues exposed to 0, 3, 15 Gy X-ray, DNAs from X-ray irradiated cells with modified nanoparticles move a longer distance than those from cells.

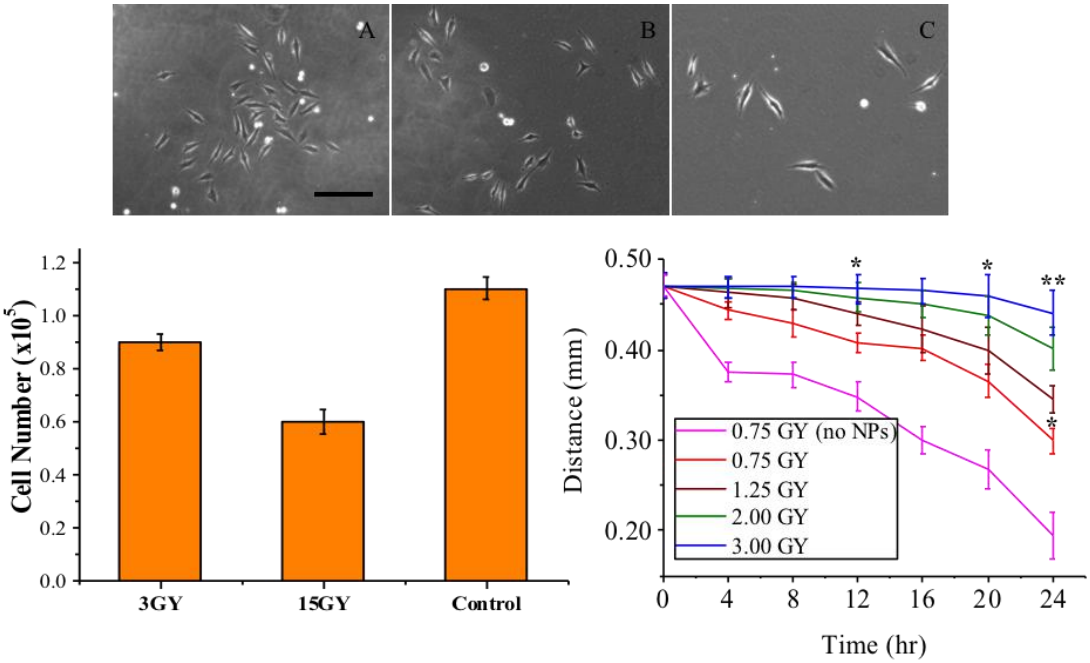

Figure 29: 3D microtissues migration in different thickness of collagen (A). 3D microtissues migration in different concentration of collagen (B). The spheoid

diameter depent on the time from day1 to day3 in different concentration of collagen (C).

5.0 Conclusions

This research has demonstrated the concept of using radiation damage of cancer cells in 3D microtissues. The enhanced radiation damage is confirmed at single cell level, chromosome and protein level by using HaloChip assay, micronucleus assay and measuring the expression of γ-H2AX protein, respectively. HaloChip assay has confirmed that microneedles can cause more DNA damage upon X-ray radiation. Micronucleus assay shows that cells of microtissues radiated with larger dose of X-ray will generate more micronucleus. The increased fluorescence signal of DNA repair protein (γ-H2AX) indicates that irradiation can enhance DNA double strand break in cells. More cells can be killed due to the effect of X-ray radiation. a large number of microtissues can be analyzed at once on each chip using this method. Such a high-density single- microtissue assay platform could be very useful for high-throughput gene library screening of tissues expressing library genes and for high sensitivity detection of extremely rare microtissues such as circulating tumor cells in peripheral blood. The single- microtissue array on a collagen surface presented here is easily customizable for different research purposes, and may be useful for unique high-throughput analysis of various biological phenomena such as cellular and tissue network formation and intercellular events. This study has demonstrated the use of cancer cell radiation injury in three-dimensional tissue. The enhanced radiation damage was confirmed at the level of individual cells, chromosome and protein levels by using HaloChip assay, micronuclear assay and measurement of the expression of cg-h2ax proteins, respectively. The HaloChip experiment confirmed that microneedles could cause more DNA damage in x-rays. Micro - nuclear experiments showed that microstructure cells with large doses of x -

rays produced more micronucleus. The increase of the fluorescence signal of DNA repair protein (-h2ax) indicates that irradiation can enhance the double strand fracture of cell DNA. Because of the effects of X-ray radiation, more cells are killed. Using this method, a large number of microstructures can be analyzed at once on each chip. The high density of single organization analysis platform for high throughput screening gene pool of gene expression library and extremely rare for micro organizations such as circulating tumor cells in peripheral blood of high sensitivity testing is very useful. Shown here in single layer on the surface of the collagen tissue array can be easily customized, used for different research purposes, and may contribute to the unique high throughput analysis of various biological phenomena, such as between the cells and the formation of the network and events. Three-dimensional microstructure is generated by the control size and shape of agedmicrowell array. Three-dimensional microstructure is used as an intermediate model between two-dimensional culture and animal models to assess radiation induced cell and DNA damage. The radiation damage of cells in three-dimensional microstructure was studied in different experiments. X-ray irradiation had different effects on the growth rate, cell vitality and protein expression of three-dimensional microstructure and two-dimensional culture cells. The work has established a way to test patients' tumor cells for better radiosensitivity tests to simulate patients' reactions during X-ray therapy. A new method for simulating tumor migration and invasion of 3d conditions was established by preparing cell clusters in collagen gel matrix. Gold nanoparticles modified with polyethylene glycol (PEG) and cell penetrating peptide (CPP) effectively delay the migration of cancer cells under X-ray irradiation. Nanoparticles can be internalized into cells. The synergistic effect between nanoparticles

and ionizing radiation affects the proteins responsible for migration, resulting in the destruction of the intracellular matrix, thereby reducing cell mobility. The internalized nanoparticles and radiation can also cause the imbalance of the cell microenvironment, promoting cell death through apoptosis. At the molecular level, the internalized nanoparticles can produce reactive oxygen species (ROS) in the cancer cells under X-ray exposure, causing DNA damage in cancer cells. Therefore, a large number of microstructures can be analyzed in this way on each chip. The high density of single organization analysis platform for high-throughput gene pool of screening, gene expression library and extremely rare for micro organizations such as circulating tumor cells in peripheral blood of high sensitivity testing is very useful. Shown here in single layer on the surface of the collagen tissue array can be easily customized, used for different research purposes, and may contribute to the unique high throughput analysis of various biological phenomena, such as between the cells and the formation of the network and events.

6.0 Recommendations

So far, a 3D microtissue has been made and used to study viability after irradiation. Specifically, future work will address the following aims:

6.1 Focus #1 The Mechanical Properties of 3D Microtissues

6.1.1 Aim #1.1

The tension is important in the research of 3D microtissue, it also related with the tissue morphogenesis, tumor growth cell metastasis as well as fibrosis. Cell-derived tension depends strongly on the mechanical environment. The rigidity of the medium in which the cells are found has been shown to influence cell division, differentiation, and apoptosis. In the next future work, combining experimental and mathematical models, we will check what can affect the cell-derived tension. Also, to check whether the tension can be controlled by varying the amount of extracellular matrix in the tissue, we will use the stiffness of the constraining structure.

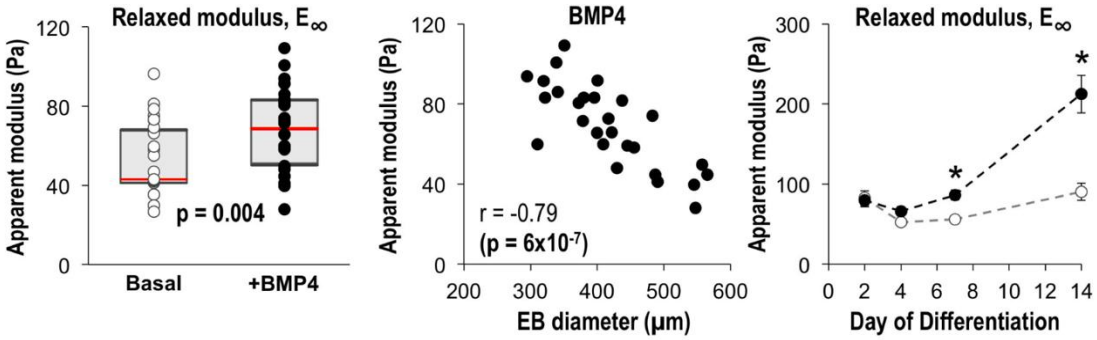

Figure 30: Dynamic modulation of 3D microtissues mechanical properties.

6.2 Focus #2 Animal test of 3D stem cells

6.2.1 Aim #1.1

The cells will be isolated from fetal human tissue obtained after elective termination of normal 18 to 24 week pregnancies. It requires 2–4 h and presents a method

for injecting tumor cells, cancer stem cells or dispersed biopsy material into subcutaneous or orthotropic locations within recipient mice. The tumor cells as well as the biopsy will be mixed with basement membrane matrix proteins (like CultrexBME or Matrigel) at 4 °C and then injected into recipient animals at preferred anatomical sites. Tumor cells can also be co-injected with additional cell types, such as fibroblasts, stromal cells, endothelial cells and so on. We will detect the difference between 2D and 3D microtissues in vivo situation.

7.0 References

1. Aminuddin, A. and P.Y. Ng, Promising Druggable Target in Head and Neck Squamous Cell Carcinoma: Wnt Signaling. Front Pharmacol, 2016. **7**: p. 244.
2. Abou-Elkacem, L., et al., Ultrasound Molecular Imaging of the Breast Cancer Neovasculature using Engineered Fibronectin Scaffold Ligands: A Novel Class of Targeted Contrast Ultrasound Agent. Theranostics, 2016. **6**(11): p. 1740-52.
3. Agboola, A.O., et al., Tumour cell membrane laminin expression is associated with basal-like phenotype and poor survival in Nigerian breast cancer. Malays J Pathol, 2016. **38**(2): p. 83-92.
4. Akay, B.N., et al., Basosquamous carcinoma: Dermoscopic clues to diagnosis. J Dermatol, 2016.
5. Al-Eisawi, Z., et al., Changes in the in vitro activity of platinum drugs when administered in two aliquots. BMC Cancer, 2016. **16**: p. 688.
6. Almendros, I., et al., Tumor Cell Malignant Properties Are Enhanced by Circulating Exosomes in Sleep Apnea. Chest, 2016.

7. Al-Saran, N., et al., Zinc enhances CDKN2A, pRb1 expression and regulates functional apoptosis via upregulation of p53 and p21 expression in human breast cancer MCF-7 cell. Environ Toxicol Pharmacol, 2016. **47**: p. 19-27.

8. Anderson, S., et al., MYC-nick promotes cell migration by inducing fascin expression and Cdc42 activation. Proc Natl Acad Sci U S A, 2016. **113**(37): p. E5481-90.

9. Arenas Valencia, C., et al., Hereditary leiomyomatosis and renal cell cancer syndrome: identification and clinical characterization of a novel mutation in the FH gene in a Colombian family. Fam Cancer, 2016.

10. Bano, S., et al., Microwave-assisted green synthesis of superparamagnetic nanoparticles using fruit peel extracts: surface engineering, T 2 relaxometry, and photodynamic treatment potential. Int J Nanomedicine, 2016. **11**: p. 3833-48.

11. Barbieri, C.E., et al., The Emergence of Precision Urologic Oncology: A Collaborative Review on Biomarker-driven Therapeutics. Eur Urol, 2016.

12. Barrozo, R.M., et al., CagY Is an Immune-Sensitive Regulator of the Helicobacter pylori Type IV Secretion System. Gastroenterology, 2016.

13. Bent, E.H., L.A. Gilbert, and M.T. Hemann, A senescence secretory switch mediated by PI3K/AKT/mTOR activation controls chemoprotective endothelial secretory responses. Genes Dev, 2016. **30**(16): p. 1811-21.

14. Bersani, F., et al., Deep Sequencing Reveals a Novel miR-22 Regulatory Network with Therapeutic Potential in Rhabdomyosarcoma. Cancer Res, 2016. **76**(20): p. 6095-6106.

15. Bertheloot, D. and E. Latz, HMGB1, IL-1alpha, IL-33 and S100 proteins: dual-function alarmins. Cell Mol Immunol, 2016.

16. Beyranvand Nejad, E., et al., Tumor Eradication by Cisplatin Is Sustained by CD80/86-Mediated Costimulation of CD8+ T Cells. Cancer Res, 2016. **76**(20): p. 6017-6029.

17. Bhatia, M., et al., Expression of the thioredoxin system in an in vivo-like cancer cell environment upon auranofin treatment. Eur J Cell Biol, 2016. **95**(10): p. 378-388.

18. Bliss, S.A., et al., Mesenchymal Stem Cell-Derived Exosomes Stimulate Cycling Quiescence and Early Breast Cancer Dormancy in Bone Marrow. Cancer Res, 2016. **76**(19): p. 5832-5844.

19. Bosco, M.C., F. Raggi, and L. Varesio, Therapeutic Potential of Targeting TREM-1 in Inflammatory Diseases and Cancer. Curr Pharm Des, 2016.

20. Bosse, K., et al., Mass spectrometry-based secretome analysis of non-small cell lung cancer cell lines. Proteomics, 2016.

21. Burness, C.B. and S.T. Duggan, Trifluridine/Tipiracil: A Review in Metastatic Colorectal Cancer. Drugs, 2016. **76**(14): p. 1393-402.

22. Cappuzzo, F., et al., Efficacy and safety of rechallenge treatment with gefitinib in patients with advanced non-small cell lung cancer. Lung Cancer, 2016. **99**: p. 31-7.

23. Caputo, P.A., et al., Cryoablation versus Partial Nephrectomy for Clinical T1b Renal Tumors: A Matched Group Comparative Analysis. Eur Urol, 2016.

24. Foolen, J., et al., Full-Length Fibronectin Drives Fibroblast Accumulation at the Surface of Collagen Microtissues during Cell-Induced Tissue Morphogenesis. PLoS One, 2016. **11**(8): p. e0160369.

25. Lee, G., et al., Reproducible Construction of Surface Tension-Mediated Honeycomb Concave Microwell Arrays for Engineering of 3D Microtissues with Minimal Cell Loss. PLoS One, 2016. **11**(8): p. e0161026.

26. Huber, J.M., et al., Evaluation of assays for drug efficacy in a three-dimensional model of the lung. J Cancer Res Clin Oncol, 2016. **142**(9): p. 1955-66.

27. Vantangoli, M.M., et al., Estradiol Exposure Differentially Alters Monolayer versus Microtissue MCF-7 Human Breast Carcinoma Cultures. PLoS One, 2016. **11**(7): p. e0157997.

28. Anastasov, N., et al., A 3D-microtissue-based phenotypic screening of radiation resistant tumor cells with synchronized chemotherapeutic treatment. BMC Cancer, 2015. **15**: p. 466.

29. Asthana, A. and W.S. Kisaalita, Microtissue size and hypoxia in HTS with 3D cultures. Drug Discov Today, 2012. **17**(15-16): p. 810-7.

30. Asthana, A. and W.S. Kisaalita, Molecular basis for cytokine biomarkers of complex 3D microtissue physiology in vitro. Drug Discov Today, 2016. **21**(6): p. 950-61.

31. Chen, A.A., G.H. Underhill, and S.N. Bhatia, Multiplexed, high-throughput analysis of 3D microtissue suspensions. Integr Biol (Camb), 2010. **2**(10): p. 517-27.

32. Kelm, J.M., et al., 3D microtissue formation of undifferentiated bone marrow mesenchymal stem cells leads to elevated apoptosis. Tissue Eng Part A, 2012. **18**(7-8): p. 692-702.

33. Kermanizadeh, A., et al., Hepatic toxicology following single and multiple exposure of engineered nanomaterials utilising a novel primary human 3D liver microtissue model. Part Fibre Toxicol, 2014. **11**: p. 56.

34. Legant, W.R., C.S. Chen, and V. Vogel, Force-induced fibronectin assembly and matrix remodeling in a 3D microtissue model of tissue morphogenesis. Integr Biol (Camb), 2012. **4**(10): p. 1164-74.

35. Muoth, C., et al., A 3D co-culture microtissue model of the human placenta for nanotoxicity assessment. Nanoscale, 2016. **8**(39): p. 17322-17332.

36. Rimann, M., et al., An in vitro osteosarcoma 3D microtissue model for drug development. J Biotechnol, 2014. **189**: p. 129-35.

37. Thoma, C.R., et al., A high-throughput-compatible 3D microtissue co-culture system for phenotypic RNAi screening applications. J Biomol Screen, 2013. **18**(10): p. 1330-7.

38. Weltin, A., et al., Accessing 3D microtissue metabolism: Lactate and oxygen monitoring in hepatocyte spheroids. Biosens Bioelectron, 2016. **87**: p. 941-948.

39. West, A.R., et al., Development and characterization of a 3D multicell microtissue culture model of airway smooth muscle. Am J Physiol Lung Cell Mol Physiol, 2013. **304**(1): p. L4-16.

40. Marsano, A., et al., Cyclic Uniaxial Strain on a Chip: a Novel Platform to Generate Functional 3D Cardiac Microtissue. Tissue Engineering Part A, 2015. **21**: p. S312-S312.

41. Thong, K.T., C.F. Soon, and K.S. Tee, The Effects of Enzyme to the Dissociation of Cells in Monolayer and 3D Microtissue on the Liquid Crystal Substrate. 5th International Conference on Biomedical Engineering in Vietnam, 2015. **46**: p. 231-234.

42. Sakar, M., et al., Quantifying Collective Cell Migration and Cell-Generated Mechanical Forces in a 3D Microtissue Model of Wound Healing. Tissue Engineering Part A, 2014. **20**: p. S36-S36.

43. Beauchamp, P., et al., A human 3D myocardial microtissue model for cardiotoxicity testing. Toxicology Letters, 2013. **221**: p. S137-S138.

44. Zuppinger, C., et al., Development of a 3D-microtissue model for testing cardiotoxicity based on human-induced pluripotent stem cells. Journal of Pharmacological and Toxicological Methods, 2013. **68**(1): p. E26-E26.

45. Anastasov, N., et al., Identification of compounds modifying radiation-therapy using a 3D-microtissue technology. Cancer Research, 2013. **73**(8).

46. Waldhauer, I., et al., Development of 3D microtissue models to study the activity of novel tumor-targeted immunotherapeutics. Cancer Research, 2013. **73**(8).

47. Schon, B.S., et al., Validation of a high-throughput microtissue fabrication process for 3D assembly of tissue engineered cartilage constructs. Cell and Tissue Research, 2012. **347**(3): p. 629-642.

48. Ma, C., et al., Pneumatic-aided micro-molding for flexible fabrication of homogeneous and heterogeneous cell-laden microgels. Lab Chip, 2016. **16**(14): p. 2609-17.

49. Kang, J., et al., Mini-pillar array for hydrogel-supported 3D culture and high-content histologic analysis of human tumor spheroids. Lab Chip, 2016. **16**(12): p. 2265-76.

50. Schon, B.S., G.J. Hooper, and T.B. Woodfield, Modular Tissue Assembly Strategies for Biofabrication of Engineered Cartilage. Ann Biomed Eng, 2016.

51. Soon, C.F., et al., A scaffoldless technique for self-generation of three-dimensional keratinospheroids on liquid crystal surfaces. Biotech Histochem, 2016. **91**(4): p. 283-95.

52. Zhao, R.G., C.S. Chen, and D.H. Reich, Force-driven evolution of mesoscale structure in engineered 3D microtissues and the modulation of tissue stiffening. Biomaterials, 2014. **35**(19): p. 5056-5064.

53. Choi, J.K., et al., The crucial role of mechanical heterogeneity in regulating follicle development and ovulation with engineered ovarian microtissue. Biomaterials, 2014. **35**(19): p. 5122-5128.

54. Sridhar, A., et al., Microstamped Petri Dishes for Scanning Electrochemical Microscopy Analysis of Arrays of Microtissues. Plos One, 2014. **9**(4).

55. Dereli-Korkut, Z., et al., Three Dimensional Microfluidic Cell Arrays for ex Vivo Drug Screening with Mimicked Vascular Flow. Analytical Chemistry, 2014. **86**(6): p. 2997-3004.

56. Kinney, M.A., R. Saeed, and T.C. McDevitt, Mesenchymal morphogenesis of embryonic stem cells dynamically modulates the biophysical microtissue niche. Scientific Reports, 2014. **4**.

57. Altmann, B., et al., Differences in morphogenesis of 3D cultured primary human osteoblasts under static and microfluidic growth conditions. Biomaterials, 2014. **35**(10): p. 3208-3219.

58. van Spreeuwel, A.C.C., et al., The influence of matrix (an)isotropy on cardiomyocyte contraction in engineered cardiac microtissues. Integrative Biology, 2014. **6**(4): p. 422-429.

59. Wang, L., et al., Engineering Three-Dimensional Cardiac Microtissues for Potential Drug Screening Applications. Current Medicinal Chemistry, 2014. **21**(22): p. 2497-2509.

60. Ramade, A., et al., Microfabrication of a Platform to Measure and Manipulate the Mechanics of Engineered Microtissues. Micropatterning in Cell Biology, Pt C, 2014. **121**: p. 191-+.

61. Thavandiran, N., et al., Design and formulation of functional pluripotent stem cell-derived cardiac microtissues. Proceedings of the National Academy of Sciences of the United States of America, 2013. **110**(49): p. E4698-E4707.

62. Qiao, Y., J.C. An, and L.Y. Ma, Single Cell Array Based Assay for in Vitro Genotoxicity Study of Nanomaterials. Analytical Chemistry, 2013. **85**(8): p. 4107-4112.

63. Zhao, R.G., et al., Decoupling Cell and Matrix Mechanics in Engineered Microtissues Using Magnetically Actuated Microcantilevers. Advanced Materials, 2013. **25**(12): p. 1699-1705.

64. Li, C.Y., et al., Flow-based pipeline for systematic modulation and analysis of 3D tumor microenvironments. Lab on a Chip, 2013. **13**(10): p. 1969-1978.

65. Hsu, Y.H., et al., Full range physiological mass transport control in 3D tissue cultures. Lab on a Chip, 2013. **13**(1): p. 81-89.

66. Messner, S., et al., Multi-cell type human liver microtissues for hepatotoxicity testing. Archives of Toxicology, 2013. **87**(1): p. 209-213.

67. Langenbach, F., et al., Scaffold-free microtissues: differences from monolayer cultures and their potential in bone tissue engineering. Clinical Oral Investigations, 2013. **17**(1): p. 9-17.

68. Schurle, S., et al., Three-dimensional, automated magnetic biomanipulation with subcellular resolution. 2013 Ieee International Conference on Robotics and Automation (Icra), 2013: p. 1452-1457.

69. Luo, Y., et al., Three-Dimensional Microtissue Assay for High-Throughput Cytotoxicity of Nanoparticles. Analytical Chemistry, 2012. **84**(15): p. 6731-6738.

70. Xu, F., et al., Release of Magnetic Nanoparticles from Cell-Encapsulating Biodegradable Nanobiomaterials. Acs Nano, 2012. **6**(8): p. 6640-6649.

71. Kabiri, M., et al., 3D mesenchymal stem/stromal cell osteogenesis and autocrine signalling. Biochemical and Biophysical Research Communications, 2012. **419**(2): p. 142-147.

72. Sakar, M.S., et al., Formation and optogenetic control of engineered 3D skeletal muscle bioactuators. Lab on a Chip, 2012. **12**(23): p. 4976-4985.

73. Kunstar, A., et al., Raman Microspectroscopy: A Noninvasive Analysis Tool for Monitoring of Collagen-Containing Extracellular Matrix Formation in a Medium-Throughput Culture System. Tissue Engineering Part C-Methods, 2011. **17**(7): p. 737-744.

74. Urciuolo, F., et al., Effect of Process Conditions on the Growth of Three-Dimensional Dermal-Equivalent Tissue Obtained by Microtissue Precursor Assembly. Tissue Engineering Part C-Methods, 2011. **17**(2): p. 155-164.

75. Bao, B., et al., Connexon-mediated cell adhesion drives microtissue self-assembly. Faseb Journal, 2011. **25**(1): p. 255-264.

76. Li, C.Y., et al., DNA-templated assembly of droplet-derived PEG microtissues. Lab on a Chip, 2011. **11**(17): p. 2967-2975.

77. Sevilla, C.A., D. Dalecki, and D.C. Hocking, Extracellular Matrix Fibronectin Stimulates the Self-Assembly of Microtissues on Native Collagen Gels. Tissue Engineering Part A, 2010. **16**(12): p. 3805-3819.

78. Otsuka, H., Nanofabrication of Nonfouling Surfaces for Micropatterning of Cell and Microtissue. Molecules, 2010. **15**(8): p. 5525-5546.

79. Kelm, J.M., et al., A novel concept for scaffold-free vessel tissue engineering: Self-assembly of microtissue building blocks. Journal of Biotechnology, 2010. **148**(1): p. 46-55.

80. Nichol, J.W., et al., Cell-laden microengineered gelatin methacrylate hydrogels. Biomaterials, 2010. **31**(21): p. 5536-5544.

81. Yang, Z.H., et al., A Novel Possible Strategy Based on Self-Assembly Approach to Achieve Complete Periodontal Regeneration. Artificial Organs, 2010. **34**(7): p. 603-U19.

82. Youssef, J., et al., Micromolded Nonadhesive Hydrogels for the Self-Assembly of Scaffold-Free 3D Cellular Microtissues. Methods in Bioengineering: 3d Tissue Engineering, 2010: p. 151-166.

83. Garzoni, L.R., et al., Dissecting coronary angiogenesis: 3D co-culture of cardiomyocytes with endothelial or mesenchymal cells. Experimental Cell Research, 2009. **315**(19): p. 3406-3418.

84. Legant, W.R., et al., Microfabricated tissue gauges to measure and manipulate forces from 3D microtissues. Proceedings of the National Academy of Sciences of the United States of America, 2009. **106**(25): p. 10097-10102.

85. Rago, A.P., D.M. Dean, and J.R. Morgan, Controlling Cell Position in Complex Heterotypic 3D Microtissues by Tissue Fusion. Biotechnology and Bioengineering, 2009. **102**(4): p. 1231-1241.

86. Dean, D.M., A.P. Rago, and J.R. Morgan, Fibroblast Elongation and Dendritic Extensions in Constrained Versus Unconstrained Microtissues. Cell Motility and the Cytoskeleton, 2009. **66**(3): p. 129-141.

87. Rago, A.P., P.R. Chai, and J.R. Morgan, Encapsulated Arrays of Self-Assembled Microtissues: An Alternative to Spherical Microcapsules. Tissue Engineering Part A, 2009. **15**(2): p. 387-395.

88. Yates, C., et al., Novel three-dimensional organotypic liver bioreactor to directly visualize early events in metastatic progression. Advances in Cancer Research, Vol 97, 2007. **97**: p. 225-+.

89. Kelm, J.M., et al., Design and characterization of cardiomyocyte-derived microtissues. Animal Cell Technology Meets Genomics, 2005: p. 213-219.

90. Bennett, K.G., et al., Treatment of Keloids With Excision and Adjuvant Radiation: A Single Center Experience and Review of the Literature. Ann Plast Surg, 2016.

91. Granato, F., et al., PET-CT as an Alternative to Fiducial Markers Guidance in Liver Metastasis Treatment. Clin Nucl Med, 2016.

92. Kingsmore, K.M., et al., Interstitial flow differentially increases patient-derived glioblastoma stem cell invasion via CXCR4, CXCL12, and CD44-mediated mechanisms. Integr Biol (Camb), 2016.

93. Verma, V., A.C. Moreno, and S.H. Lin, Advances in Radiotherapy Management of Esophageal Cancer. J Clin Med, 2016. **5**(10).

94. Suh, D.H., et al., Major clinical research advances in gynecologic cancer in 2015. J Gynecol Oncol, 2016. **27**(6): p. e53.

95. McGarry, S.D., et al., Magnetic Resonance Imaging-Based Radiomic Profiles Predict Patient Prognosis in Newly Diagnosed Glioblastoma Before Therapy. Tomography, 2016. **2**(3): p. 223-228.

96. Muz, B., et al., The role of hypoxia in cancer progression, angiogenesis, metastasis, and resistance to therapy. Hypoxia (Auckl), 2015. **3**: p. 83-92.

97. D'Souza, N.M., et al., Combining Radiation Therapy with Immune Checkpoint Blockade for Central Nervous System Malignancies. Front Oncol, 2016. **6**: p. 212.

98. Wang, B., S.J. Walsh, and M.W. Saif, Pancytopenia and Severe Gastrointestinal Toxicities Associated with 5-Fluorouracil in a Patient with Thymidylate Synthase (TYMS) Polymorphism. Cureus, 2016. 8(9): p. e798.

99. Sasaki, A., S. Miyazaki, and T. Hori, Extracranial Facial Nerve Schwannoma Treated by Hypo-fractionated CyberKnife Radiosurgery. Cureus, 2016. 8(9): p. e797.

100. Zettervall, S.L., et al., Clinical presentation, management, follow-up, and outcomes of isolated celiac and superior mesenteric artery dissections. J Vasc Surg, 2016.

101. Simmonds, J.C. and E.E. Rebeiz, Surgical resection of sinonasal hemangiopericytoma involving anterior skull base: case reports and literature review. Am J Otolaryngol, 2016.

102. Le, J., Oncogenic gamma Herpesviruses EBV and HHV8 in Kidney Transplantation. Semin Nephrol, 2016. 36(5): p. 362-371.

103. Madubata, C.C., et al., Comparing treatment and outcomes of ductal carcinoma in situ among women in Missouri by race. Breast Cancer Res Treat, 2016.

104. Miyamura, K., et al., Switching to nilotinib in patients with chronic myeloid leukemia in chronic phase with molecular suboptimal response to frontline imatinib: SENSOR final results and BIM polymorphism substudy. Leuk Res, 2016. **51**: p. 11-18.

105. Darwish, A.D., et al., Breast cancer in women aging 35 years old and younger: The Egyptian National Cancer Institute (NCI) experience. Breast, 2016. **31**: p. 1-8.

106. Rey, S., et al., Molecular Targeting of Hypoxia in Radiotherapy. Adv Drug Deliv Rev, 2016.

107. Vantangoli, M.M., et al., Morphologic effects of estrogen stimulation on 3D MCF-7 microtissues. Toxicol Lett, 2016. **248**: p. 1-8.

108. Falkenberg, N., et al., Three-dimensional microtissues essentially contribute to preclinical validations of therapeutic targets in breast cancer. Cancer Med, 2016. **5**(4): p. 703-10.

109. Ma, C., et al., On-Chip Construction of Liver Lobule-like Microtissue and Its Application for Adverse Drug Reaction Assay. Anal Chem, 2016. **88**(3): p. 1719-27.

110. Brennan, J.R. and D.C. Hocking, Cooperative effects of fibronectin matrix assembly and initial cell-substrate adhesion strength in cellular self-assembly. Acta Biomater, 2016. **32**: p. 198-209.

111. Agarkova, I., et al., Organotypic 3D in vitro microtissue models for cardiac and liver safety assessment. Journal of Pharmacological and Toxicological Methods, 2014. **70**(3): p. 328-328.

112. Richert, L., et al., Cytotoxicity evaluation using cryopreserved primary human hepatocytes in various culture formats. Toxicology Letters, 2016. **258**: p. 207-215.

113. Chen, Z.W., et al., Lung Microtissue Array to Screen the Fibrogenic Potential of Carbon Nanotubes. Scientific Reports, 2016. **6**.

114. Kalman, B., C. Picart, and T. Boudou, Quick and easy microfabrication of T-shaped cantilevers to generate arrays of microtissues. Biomedical Microdevices, 2016. **18**(3).

115. Schell, J.Y., et al., Harnessing cellular-derived forces in self-assembled microtissues to control the synthesis and alignment of ECM. Biomaterials, 2016. **77**: p. 120-129.

116. Prodanov, L., et al., Long-term maintenance of a microfluidic 3D human liver sinusoid. Biotechnology and Bioengineering, 2016. **113**(1): p. 241-246.

117. Thong, K.T., et al., Development of a Microfluidic Vibrational Cleaning System for Cleaning Microtissues. International Conference for Innovation in Biomedical Engineering and Life Sciences, Icibel2015, 2016. **56**: p. 155-158.

118. Beachley, V.Z., et al., Tissue matrix arrays for high-throughput screening and systems analysis of cell function. Nature Methods, 2015. **12**(12): p. 1197-+.

119. Kabadi, P.K., et al., Into the depths: Techniques for in vitro three-dimensional microtissue visualization. Biotechniques, 2015. **59**(5): p. 279-285.

120. Frimat, J.P., et al., Advances in 3D neuronal cell culture. Journal of Vacuum Science & Technology B, 2015. **33**(6).

121. McCarty, W.J., et al., Layer-by-layer Collagen Deposition in Microfluidic Devices for Microtissue Stabilization. Jove-Journal of Visualized Experiments, 2015(103).

122. Futrega, K., et al., The microwell-mesh: A novel device and protocol for the high throughput manufacturing of cartilage microtissues. Biomaterials, 2015. **62**: p. 1-12.

123. Kim, J.Y., et al., 3D spherical microtissues and microfluidic technology for multi-tissue experiments and analysis. Journal of Biotechnology, 2015. **205**: p. 24-35.

124. Nam, K.H., et al., Biomimetic 3D Tissue Models for Advanced High-Throughput Drug Screening. Jala, 2015. **20**(3): p. 201-215.

125. Lu, Y.C., et al., Designing compartmentalized hydrogel microparticles for cell encapsulation and scalable 3D cell culture. Journal of Materials Chemistry B, 2015. **3**(3): p. 353-360.

126. Yazdi, S.R., et al., Microfluidic Hanging-Drop Platform for Parallel Closed-Loop Multi-Tissue Experiments. 2015 28th Ieee International Conference on Micro Electro Mechanical Systems (Mems 2015), 2015: p. 535-538.

127. Alonzo, L.F., et al., Microfluidic device to control interstitial flow-mediated homotypic and heterotypic cellular communication. Lab on a Chip, 2015. **15**(17): p. 3521-3529.

128. Yazdi, S.R., et al., Adding the 'heart' to hanging drop networks for microphysiological multi-tissue experiments. Lab on a Chip, 2015. **15**(21): p. 4138-4147.

129. Xu, F., et al., A microfabricated magnetic actuation device for mechanical conditioning of arrays of 3D microtissues. Lab on a Chip, 2015. **15**(11): p. 2496-2503.

130. Naderi, N., et al., Adipogenic differentiation of adipose-derived stem cells in 3-dimensional spheroid cultures (microtissue): Implications for the reconstructive surgeon. Journal of Plastic Reconstructive and Aesthetic Surgery, 2014. **67**(12): p. 1726-1734.

131. Repin, V.S., et al., 3D-Technology of the Formation and Maintenance of Single Dormant Microspheres from 2000 Human Somatic Cells and Their Reactivation In Vitro. Bulletin of Experimental Biology and Medicine, 2014. **158**(1): p. 137-144.

132. Liu, W., et al., Magnetically controllable 3D microtissues based on magnetic microcryogels. Lab on a Chip, 2014. **14**(15): p. 2614-2625.

133. Frey, O., et al., Reconfigurable microfluidic hanging drop network for multi-tissue interaction and analysis. Nature Communications, 2014. **5**.

134. Luo, H.Y., et al., Fabrication of viable centimeter-sized 3D tissue constructs with microchannel conduits for improved tissue properties through assembly of cell-laden microbeads. Journal of Tissue Engineering and Regenerative Medicine, 2014. **8**(6): p. 493-504.

135. Miyamoto, D.T. and R.J. Lee, Cell-free and circulating tumor cell-based biomarkers in men with metastatic prostate cancer: Tools for real-time precision medicine? Urol Oncol, 2016.

136. Spratt, D.E., et al., The American Brachytherapy Society Task Group Report: Combination of brachytherapy and external beam radiation for high-risk prostate cancer. Brachytherapy, 2016.

137. Chan, J.K., et al., The association between timing of initiation of adjuvant therapy and the survival of early stage ovarian cancer patients - An analysis of NRG oncology/gynecologic oncology group trials. Gynecol Oncol, 2016.

138. Wilkman, T., et al., A Comparison of Bone Resorption Over Time: An Analysis of the Free Scapular, Iliac Crest, and Fibular Microvascular Flaps in Mandibular Reconstruction. J Oral Maxillofac Surg, 2016.

139. Frappaz, D., et al., [Pediatric ependymomas: Current diagnosis and therapy]. Bull Cancer, 2016. **103**(10): p. 869-879.

140. Gichuhi, S., et al., Risk factors for ocular surface squamous neoplasia in Kenya: a case-control study. Trop Med Int Health, 2016.

141. Lobachevsky, P., et al., Compromized DNA repair as a basis for identification of cancer radiotherapy patients with extreme radiosensitivity. Cancer Lett, 2016. **383**(2): p. 212-219.

142. Harryman, W.L., et al., The Cohesive Metastasis Phenotype in Human Prostate Cancer. Biochim Biophys Acta, 2016. **1866**(2): p. 221-231.

143. Yang, N., et al., PIDD Mediates Radiation-Induced Microglia Activation. Radiat Res, 2016. **186**(4): p. 345-359.

144. Robin, T.P., et al., Disparities in standard of care treatment and associated survival decrement in patients with locally advanced cervical cancer. Gynecol Oncol, 2016. **143**(2): p. 319-325.

145. Zhang, N., et al., Low density lipoprotein receptor targeted doxorubicin/DNA-Gold Nanorods as a chemo- and thermo-dual therapy for prostate cancer. Int J Pharm, 2016. **513**(1-2): p. 376-386.

146. Gewirtz, D.A., et al., Tumor Cell Recovery from Senescence Induced by Radiation with PARP Inhibition. Radiat Res, 2016. **186**(4): p. 327-332.

147. Mallen-St Clair, J., et al., Human papillomavirus in oropharyngeal cancer: The changing face of a disease. Biochim Biophys Acta, 2016. **1866**(2): p. 141-150.

148. Ahmad, S., et al., Incidence of intracranial radiation necrosis following postoperative radiation therapy for sinonasal malignancies. Laryngoscope, 2016. **126**(11): p. 2445-2450.

149. Marzouki, H.Z., et al., Modification of the submandibular gland transfer procedure. Laryngoscope, 2016. **126**(11): p. 2492-2496.

150. Blasi, M.A., et al., BRACHYTHERAPY ALONE OR WITH NEOADJUVANT PHOTODYNAMIC THERAPY FOR AMELANOTIC CHOROIDAL MELANOMA: Functional Outcomes and Local Tumor Control. Retina, 2016. **36**(11): p. 2205-2212.

151. Wise, S.C., et al., Surgical salvage of recurrent vestibular schwannoma following prior stereotactic radiosurgery. Laryngoscope, 2016. **126**(11): p. 2580-2586.

152. Casas, F., et al., Intermittent versus continuous androgen deprivation therapy to biochemical recurrence after external beam radiotherapy: a phase 3 GICOR study. Clin Transl Oncol, 2016.

153. Indini, A., et al., Long-term safety of growth hormone replacement therapy after childhood medulloblastoma and PNET: it is time to set aside old concerns. J Neurooncol, 2016.

154. Marvaso, G., et al., Hadrontherapy from the Italian Radiation Oncologist point of view: face the reality. The Italian Society of Oncological Radiotherapy (AIRO) survey. Radiol Med, 2016.

155. Thottian, A.G., et al., Coughing up - Small cell carcinoma lung with gingival metastasis. J Egypt Natl Canc Inst, 2016.

156. Bibault, J.E., et al., Empowering patients for radiation therapy safety: Results of the EMPATHY study. Cancer Radiother, 2016.

157. Rah, J.E., et al., A treatment planning study of proton arc therapy for para-aortic lymph node tumors: dosimetric evaluation of conventional proton therapy, proton arc therapy, and intensity modulated radiotherapy. Radiat Oncol, 2016. **11**(1): p. 140.

158. Belles, M., et al., Exposure to low doses of 137cesium and nicotine during postnatal development modifies anxiety levels, learning, and spatial memory performance in mice. Food Chem Toxicol, 2016. **97**: p. 82-88.

159. Hwang, J.A., et al., Clinical Implications of Isolated Bone Failure Without Systemic Disease Progression During EGFR-TKI Treatment. Clin Lung Cancer, 2016. **17**(6): p. 573-580 e1.

160. Berriochoa, C., et al., Stereotactic Body Radiotherapy for T3N0 Lung Cancer With Chest Wall Invasion. Clin Lung Cancer, 2016. **17**(6): p. 595-601.

161. Hao, C., et al., Accumulation of RNA-dependent protein kinase (PKR) in the nuclei of lung cancer cells mediates radiation resistance. Oncotarget, 2016. **7**(25): p. 38235-38242.

162. Park, B.D., T.G. Kim, and J.E. Kim, Dosimetric impact of intermediate dose calculation for optimization convergence error. Oncotarget, 2016. **7**(25): p. 37589-37598.

163. Loganadane, G., et al., Stereotactic ablative radiotherapy for early stage non-small cell lung cancer: A critical literature review of predictive factors of relapse. Cancer Treat Rev, 2016. **50**: p. 240-246.

164. Bishay, V.L., et al., Transradial Approach for Hepatic Radioembolization: Initial Results and Technique. AJR Am J Roentgenol, 2016. **207**(5): p. 1112-1121.

165. Wei, K.C., et al., Management of fluoroscopy-induced radiation ulcer: One-stage radical excision and immediate reconstruction. Sci Rep, 2016. **6**: p. 35875.

166. Pilewskie, M., et al., Women with Low-Risk DCIS Eligible for the LORIS Trial After Complete Surgical Excision: How Low Is Their Risk After Standard Therapy? Ann Surg Oncol, 2016.

167. Gocgun, Y., Simulation-based approximate policy iteration for dynamic patient scheduling for radiation therapy. Health Care Manag Sci, 2016.

168. South, A., et al., Estimating the Impact of Randomised Control Trial Results on Clinical Practice: Results from a Survey and Modelling Study of Androgen Deprivation Therapy plus Radiotherapy for Locally Advanced Prostate Cancer. Eur Urol Focus, 2016. **2**(3): p. 276-283.

169. Daimon, T., T. Kosaka, and M. Oya, A metastatic castration resistant prostate cancer patient with multiple bone metastases has durable biochemical and radiological response to docetaxel chemotherapy. Am J Clin Exp Urol, 2016. **4**(2): p. 28-31.

170. Langen, B., et al., Microarray Studies on 211At Administration in BALB/c Nude Mice Indicate Systemic Effects on Transcriptional Regulation in Non-Thyroid Tissues. J Nucl Med, 2016.

171. Son, K., et al., IMAGING DOSE OF HUMAN ORGANS FROM kV-CBCT IN IMAGE-GUIDED RADIATION THERAPY. Radiat Prot Dosimetry, 2016.

172. Ekici, K., et al., Dosimetric comparison of helical tomotherapy, intensity-modulated radiation therapy, volumetric-modulated arc therapy, and 3-dimensional conformal therapy for the treatment of T1N0 glottic cancer. Med Dosim, 2016.

173. Owosho, A.A., et al., Comparison of mean radiation dose and dosimetric distribution to tooth-bearing regions of the mandible associated with proton beam radiation therapy and intensity-modulated radiation therapy for ipsilateral head and neck tumor. Oral Surg Oral Med Oral Pathol Oral Radiol, 2016. **122**(5): p. 566-571.

174. De Amorim Bernstein, K. and T. DeLaney, Chordomas and chondrosarcomas-The role of radiation therapy. J Surg Oncol, 2016. **114**(5): p. 564-569.

175. Barjaktarovic, Z., et al., Low-dose radiation differentially regulates protein acetylation and histone deacetylase expression in human coronary artery endothelial cells. Int J Radiat Biol, 2016: p. 1-9.

176. Patel, S.V., et al., Distance to the anal verge is associated with pathologic complete response to neoadjuvant therapy in locally advanced rectal cancer. J Surg Oncol, 2016. **114**(5): p. 637-641.

177. Schneider, A.L., et al., Ability of the National Surgical Quality Improvement Program Risk Calculator to Predict Complications Following Total Laryngectomy. JAMA Otolaryngol Head Neck Surg, 2016. **142**(10): p. 972-979.

178. Kim, S.S., et al., Preoperative FOLFIRINOX for borderline resectable pancreatic cancer: Is radiation necessary in the modern era of chemotherapy? J Surg Oncol, 2016. **114**(5): p. 587-596.

179. Sciacero, P., et al., The role of radiation therapy in vulvar cancer: review of the current literature. Tumori, 2016: p. 0.

180. Alamri, Y., et al., Salvage surgery in patients with recurrent or residual squamous cell carcinoma of the anus. Eur J Surg Oncol, 2016. **42**(11): p. 1687-1692.

181. Tuljapurkar, V., et al., The Indian scenario of head and neck oncology - Challenging the dogmas. South Asian J Cancer, 2016. **5**(3): p. 105-10.

182. Matsuura, T., et al., Clinical outcomes of IMRT planned with or without PET/CT simulation for patients with pharyngeal cancers. Int J Clin Oncol, 2016.

183. G. Tarantino, M. N. D. Di Minno and D. Capone, World J. Gastroenterol., 2009, 15, 2817.

184. G. Luo, T. Guenthner, L.-S. Gan and W. G. Humphreys, Curr. Drug Metab., 2004, 5, 483–505.

185. N. J. Hewitt, M. J. Gómez echón, J B H uston, D H llifax, H S B own, P M ur el, J G K nna, L G stavsson, C L hmann a d C S onberg, D ug M tab. R v., 2 07, 3 , 1 9–234.

186. S. Zmora, R. Glicklis and S. Cohen, Biomaterials, 2002, 23, 4087–4094.

187. J. A. DiMasi, R. W. Hansen and H. G. Grabowski, J. Health Econ., 2003, 22, 151–185.

188. Z. Dereli-Korkut, H. D. Akaydin, A. H. Ahmed, X. Jiang and S. Wang, Anal. Chem., 2014, 86, 2997–3004.

189. Y. C. Toh, C. Zhang, J. Zhang, Y. M. Khong, S. Chang, D. van Noort, V. Samper, D. W. Hutmacher and H. Yu, Lab Chip, 2007, 7, 302–309.

190. P. S. Dittrich and A. Manz, Nat. Rev. Drug Discovery, 2006, 5, 210–218.

191. B. J. Kane, M. J. Zinner, M. L. Yarmush and M. Toner, Anal. Chem., 2006, 78, 4291–4298.

192. R. T. Mingoia, D. L. Nabb, C. H. Yang and X. Han, Toxicol. in Vitro, 2007, 21, 165–173.

193. R. Shrivastava, C. Delomenie, A. Chevalier, G. John, B. Ekwall, E. Walum and R. Massingham, Cell Biol. Toxicol., 1992, 8, 157–170.

194. L. Chan, S. Gosangari, K. Watkin and B. Cunningham, Apoptosis, 2007, 12, 1061.

195. W. Zhou, C. C. Chen, B. Buckland and J. Aunins, Biotechnol. Bioeng., 1997, 55, 783–792.

196. Y. Torisawa, A. Takagi, Y. Nahimoto, T. Yasukawa, H. Shiku and T. Matsue, Biomaterials, 2007, 28, 559–566.

197. J. Friedrich, R. Ebner and L. A. Kunz-Schughart, Int. J. Radiat. Biol., 2007, 83, 849–871.

198. W. Zhou, C. C. Chen, B. Buckland and J. Aunins, Biotechnol. Bioeng., 1997, 55, 783–792.

199. D. Del Duca, T. Werbowetski and R. F. Del Maestro, J. Neuro-Oncol., 2004, 67, 295–303.

200. F. Pampaloni, E. G. Reynaud and E. H. K. Stelzer, Nat. Rev. Mol. Cell Biol., 2007, 8, 839–845.

201. C. Y. Li, D. K. Wood, C. M. Hsu and S. N. Bhatia, Lab Chip, 2011, 11, 2967–2975.

202. X. Y. Wang, V. Veerappan, C. Cheng, X. Jiang, R. D. Allen, P. K. Dasgupta and S. R. Liu, J. Am. Chem. Soc., 2010, 132, 40–41.

203. G. H. Lee, J. S. Lee, X. Wang and S. H. Lee, Adv. Healthcare Mater., 2016, 5, 56–74.

204. K. H. Nam, A. S. Smith, S. Lone, S. Kwon and D. H. Kim, J. Lab. Autom., 2015, 20, 201–215.

205. V. S. Repin, I. N. Saburina, N. V. Kosheleva, A. A. Gorkun, I. M. Zurina and A. A. Kubatiev, Bull. Exp. Biol. Med., 2014, 158, 137–144.

206. J. Y. Kim, D. A. Fluri, R. Marchan, K. Boonen, S. Mohanty, P. Singh, S. Hammad, B. Landuyt, J. G. Hengstler, J. M. Kelm, A. Hierlemann and O. Frey, J. Biotechnol., 2015, 205, 24–35.

207. Kim DA, Suh EK. Defying DNA double-strand break-induced death during prophase I meiosis by temporal TAp63a phosphorylation regulation in developing mouse oocytes. Mol Cell Biol. 2014; 34: 1460-1473.

208. Polci R, Peng A, Chen PL, Riley DJ, Chen Y. NIMA-related protein kinase 1 is involved early in the ionizing radiation-induced DNA damage response. Cancer Res. 2004; 64: 8800-8803.

209. Podhorecka M, Skladanowski A, Bozko P. H2AX Phosphorylation: Its Role in DNA Damage Response and Cancer Therapy. J Nucleic Acids. 2010; 2010.

210. Kang MA, So EY, Simons AL, Spitz DR, Ouchi T. DNA damage induces reactive oxygen species generation through the H2AX-Nox1/Rac1 pathway. Cell Death Dis. 2012; 3: e249.

211. Liang SH, Clarke MF. Regulation of p53 localization. Eur J Biochem. 2001; 268: 2779-2783.